

# Solid-State NMR Techniques for the Structural Determination of Amyloid Fibrils

Jerry C.C. Chan

**Abstract** This review discusses the solid-state NMR techniques developed for the study of amyloid fibrils. Literature up to the end of 2010 has been surveyed and the materials are organized according to five categories, viz. homonuclear dipolar recoupling and polarization transfer via J-coupling, heteronuclear dipolar recoupling, correlation spectroscopy, recoupling of chemical shift anisotropy, and tensor correlation. Our emphasis is on the NMR techniques and their practical aspects. The biological implications of the results obtained for amyloid fibrils are only briefly discussed. Our main objective is to showcase the power of NMR in the study of biological unoriented solids.

**Keywords** Amyloid fibrils · Backbone torsion angle · Correlation spectroscopy · CSA · Dipolar recoupling · H/D exchange · J-coupling · Tensor correlation

## Contents

1	Introduction .....	48
2	Homonuclear Dipolar Recoupling and J-Coupling Based Techniques .....	49
2.1	Rotational Resonance .....	49
2.2	Dipolar Dephasing .....	50
2.3	Constant-Time Dipolar Dephasing .....	51
2.4	Multiple-Quantum NMR .....	55
2.5	Polarization Transfer Via Homonuclear J-Coupling .....	56
2.6	Frequency-Selective Polarization Transfer .....	57
3	Heteronuclear Dipolar Recoupling Techniques .....	58
3.1	REDOR .....	58
3.2	Frequency-Selective REDOR .....	60
3.3	DSQ-REDOR .....	61
3.4	Band-Selective TEDOR .....	62
3.5	<sup>1</sup> H–X Dipolar Couplings .....	63

---

J.C.C. Chan

Department of Chemistry, National Taiwan University, No. 1, Section 4, Roosevelt Road, Taipei, Taiwan

e-mail: chanjcc@ntu.edu.tw

4	Correlation Spectroscopy .....	64
4.1	Spectral Assignment .....	64
4.2	Distance Constraints .....	68
4.3	H/D Exchange Detected by Correlation Spectroscopy .....	69
5	Recoupling of Chemical Shift Anisotropy .....	71
5.1	Theory of ROCSA .....	71
5.2	ROCSA Spectra of Amyloid Fibrils .....	73
6	Tensor Correlation Methods .....	75
6.1	Backbone Phi-Psi Angle Determination .....	76
6.2	Backbone Psi Angle Determination .....	77
6.3	Backbone Phi Angle Determination .....	79
7	Conclusion and Outlook .....	82
	References .....	83

## 1 Introduction

Amyloid fibrils are filamentous insoluble protein aggregates closely related to many fatal neurodegenerative diseases including Alzheimer's disease, type II diabetes, Huntington's disease, and prion diseases [1, 2]. The molecular structure of amyloid fibrils is known to contain  $\beta$ -sheets that extend over the length of the fibril, created by intermolecular hydrogen bonding of  $\beta$ -strand peptide segments that run perpendicular to the fibril axis, which is commonly referred to as the cross- $\beta$  motif. It has been known for some years that the amyloid fibrils formed by peptide sequences of very different biophysical properties have many structural features in common [1]. To unravel the physical principles governing this interesting phenomenon, which can provide significant mechanistic insights into the self-assembly process of macromolecules, it is necessary to determine the molecular structures of amyloid fibrils formed by a large variety of proteins or their fragments. Since the pioneering work by Griffin and co-workers [3], solid-state NMR has been established as the major analytical tool to unravel the structural details of amyloid fibrils at the molecular level [4, 5]. Over the years, solid-state NMR studies of amyloid fibrils have been reviewed regularly [4–9, 11, 12]. Many cleverly designed solid-state NMR strategies have been developed to probe the hydrogen-bond registry of  $\beta$ -sheet layer, the spatial organization of the various  $\beta$ -sheet segments of the peptide chain, the existence of salt bridge, the side-chain–side-chain interactions, the quaternary contacts between  $\beta$ -sheet layers, the staggering of neighboring  $\beta$  strands, and the motional dynamics of the backbone. The review by Naito and Kawamura has also included a nice exposition of the interaction between amyloidogenic protein and membranes [12].

Biological solid-state NMR is such an active research field that many new techniques and notions have been reported in the past few years. It is simply beyond the scope of the present review to include all the techniques which may find fruitful applications in the study of amyloid fibrils. Given the page limit, we will only focus on the NMR techniques which have already been applied to the study of unoriented solid-state samples of amyloid fibrils. As implied from the title, our emphasis will be placed on the NMR techniques and the implications of the results obtained for

amyloid fibrils will only be briefly discussed. Our purpose is to present “what has been done” so that one may consider “what could be done.” On a more general note, we hope that the applications discussed for amyloid fibrils can showcase the power of NMR in the study of biological solids. Most of the techniques discussed are under the condition of magic-angle spinning (MAS), which consists of radiofrequency (rf) pulse sequences that are applied in synchrony with the MAS sample rotation. Our discussion is largely descriptive and will include some practical hints on the experimental aspect. For a more in-depth discussion of the techniques and theories, readers are referred to the original literature.

## 2 Homonuclear Dipolar Recoupling and J-Coupling Based Techniques

In the cross- $\beta$  structural motif, the registry of the hydrogen bonds between the  $\beta$  strands is determined by a delicate balance of multiple side-chain–side-chain interactions. Experimentally, the organization of the  $\beta$ -sheet structure can be determined by measuring the distance between two selected residues in adjacent  $\beta$  strands. Some very useful homonuclear dipolar recoupling techniques for distance measurements and spin counting will be discussed. In addition, homonuclear polarization transfer techniques mediated by the scalar spin–spin coupling (J-coupling) will also be covered in the following section. The dipolar recoupling techniques developed for homonuclear correlation spectroscopy are discussed in Sect. 4.

### 2.1 Rotational Resonance

Rotational resonance ( $R^2$ ) is the first solid-state NMR technique applied to study amyloid fibrils [3, 13–15]. One common implementation is to set the spinning frequency equal to the chemical shift difference of the spin pair of interest, say,  $I$  and  $S$ . To the lowest order, the average Hamiltonian contains the zero-quantum (ZQ) flip-flop term ( $I_+S_- + I_-S_+$ ) [16, 17]. Therefore, the density operator of the spin system would oscillate between the terms of  $I_z-S_z$  and of the ZQ coherence ( $I_+S_- - I_-S_+$ ). After a selective inversion of either polarization to the  $-z$  axis, which would maximize the initial polarization difference, the amplitude of  $I_z-S_z$  can be monitored as a function of the mixing time. From the time course of the exchange in Zeeman order, the internuclear distance could be extracted if the  $T_2$  relaxation of the ZQ coherence ( $T_2^{\text{ZQ}}$ ) is known. Usually,  $T_2^{\text{ZQ}}$  is approximated by the  $T_2$  relaxations of  $I$  and  $S$ , according to the equation  $(T_2^{\text{ZQ}})^{-1} = (T_2^I)^{-1} + (T_2^S)^{-1}$ . Interestingly, it has been suggested that  $T_2^{\text{ZQ}}$  can be measured directly in a Hahn-echo like experiment, where the ZQ coherence can be refocused by the

composite  $(\pi/2)_x - (\pi/2)_y - (\pi/2)_x$  pulse [18]. Because the chemical shift difference of the carbonyl and aliphatic regions is about 130–160 ppm, distances of the spin pairs of  $C'-C^\alpha$ ,  $C'-C^\beta$ , or  $C'-C^\gamma$  can be estimated conveniently by  $R^2$ . This strategy has been applied in the study of the fibrils formed by PrP<sub>106–126</sub> [19], where it has been shown that the fibril structure comprises a close stacking of two neighboring  $\beta$ -sheets adopting the structural motif of the class 1 steric zipper [20]. Recently, a constant-time version of the  $R^2$  experiment has been developed [21, 22], where the dynamics of the magnetization transfer is monitored as a function of the spinning frequency. This so-called rotational resonance width ( $R^2W$ ) technique has the advantage that its data analysis allows an independent extraction of the internuclear distance and the  $T_2^{ZQ}$  parameter [21, 23]. Previously, it has been shown that the fibrils formed by the peptide GNNQQNY have three different polymorphs [24]. For the fibril sample formed by a 50/50 (by mass) mixture of the peptides of [ $^{13}C'$ -Gly]-NNQQNY and [ $^{13}C^\alpha$ -Gly]-NNQQNY, the intermolecular  $^{13}C$ – $^{13}C$  distance has been determined by the technique of  $R^2W$  [25]. The results lie in the range of 4.5–4.9 Å (with an error of  $\pm 1.0$  Å), consistent with the in-register parallel  $\beta$ -sheet structure.

## 2.2 Dipolar Dephasing

The technique of dipolar recoupling with a windowless sequence (DRAWS) has been developed to recouple homonuclear dipole–dipole interaction under MAS conditions [26, 27]. The lowest-order average Hamiltonian of DRAWS is proportional to the terms of  $(I_x S_x - I_y S_y)$  and  $(3I_z S_z - I \cdot S)$ . When the transverse magnetization is allowed to evolve under DRAWS, the dephasing rate of the signal will depend on the dipolar coupling constants and the  $T_2$  relaxation. By measuring the crystalline compound of adipic acid, the upper limit of  $^{13}C$ – $^{13}C$  distances measurable by DRAWS was established to be ca. 6 Å [18]. In an early application of DRAWS to the study of amyloid fibrils, the organization of the  $\beta$ -sheet structure for A $\beta_{10–35}$  fibrils has been shown to be in-register parallel [28]. In addition, the secondary structure of the peptide monomer has been verified to adopt  $\beta$ -sheet structure by measuring the  $C'_{(i)}-C'_{(i+1)}$  distances at selected residues [18]. To mimic the spin evolution of an “infinite” long chain as anticipated for fibrils of a few microns in length, each of the spins in a linear chain was set to have two coupled neighbors [18]. In particular, the spins at the two ends are “coupled” as if they were neighbors. This implementation of periodic boundary conditions has been shown to be an effective approach to eliminate the “edge effect” [18, 29]. DRAWS can also be used to prepare a double-quantum filter (DQF) [30]. The advantage of the resulting DQF–DRAWS technique is that the dipolar coupling and the relaxation parameters can be independently extracted from the excitation profile of the DQ signal [29]. Hence, it is possible to determine accurately by DQF–DRAWS the interstrand distances in amyloid fibrils [25, 29, 31, 32]. While DRAWS is very well compensated for the effect of chemical shift anisotropy (CSA) [33], the required rf

field is 8.5 times the spinning frequency, which has precluded its application in the fast spinning regime. In addition, the implementation of windowless pulse sequences is not trivial if phase transient problems are severe. Sometimes a damping resistor has to be added in parallel to the sample coil in order to reduce the detrimental effect of phase glitches [18, 34].

The homonuclear dipolar recoupling technique of radio frequency-driven recoupling (RFDR) involves a hard  $\pi$  pulse per rotor period and its recoupling mechanism is based on the modulation of chemical shift difference [35–37]. When the delta-pulse approximation is relaxed so that the pulse width of the  $\pi$  pulse is about one-third of the rotor period, the so-called finite-pulse RFDR (fpRFDR) could selectively reintroduce the homonuclear dipole–dipole interaction under fast MAS conditions [38]. Because the recoupling mechanism of fpRFDR does not require the presence of chemical shift difference, it can be applied to study samples with a singly labeled site. For the study of amyloid fibrils, the technique of fpRFDR is usually applied in a constant-time framework (see below).

### 2.3 Constant-Time Dipolar Dephasing

To minimize the effects of various experimental imperfections such as rf inhomogeneity and  $T_2$  relaxation, it is highly desirable to design a recoupling experiment where the number of rf pulses and the total pulse sequence duration are maintained constant [39]. It has been shown that the average Hamiltonian of the fpRFDR recoupling sequence has the same operator form as the static homonuclear dipole–dipole interaction [38]. Hence, the classical WAHUHA sequence developed for homonuclear decoupling under static condition [40], viz.  $\tau - (\pi/2)_x - \tau - (\pi/2)_y - 2\tau - (\pi/2)_y - \tau - (\pi/2)_x - \tau$ , can be exploited as shown in Fig. 1 to achieve homonuclear dipolar recoupling in a constant-time manner [41]. That is, the total duration of the pulse sequence is kept constant and the effective dipolar dephasing time is varied by adjusting the positions of the WAHUHA pulses. In other words, we combine two pulse sequences which have opposite effects. While fpRFDR will reintroduce the homonuclear dipole–dipole interaction, WAHUHA will suppress it, so that the net dipolar dephasing occurs as a result of “controlled” cancellation. This technique, which has the acronym fpRFDR-CT, has been successfully applied to probe the  $\beta$ -sheet organization of amyloid fibrils [4, 42].

For the amyloid fibrils formed by proteins or polypeptides with more than 20 amino acid residues, the fibril core usually comprises in-register parallel  $\beta$ -sheets [19, 28, 43–50], although it has also been shown that a polymorph of the D23N-A $\beta$ 40 fibrils may have an antiparallel  $\beta$ -sheet structure [51]. The fpRFDR-CT technique is well suited to verify whether or not a fibril system adopts the organization of in-register parallel  $\beta$ -sheets. For a single  $\beta$ -sheet layer, significant signal dephasings of the  $C'$  and  $C^\beta$  labeled at two different residues will provide strong evidence for in-register parallel organization. In particular, shifting the hydrogen bond registry away from in-register alignment by one residue in either direction will

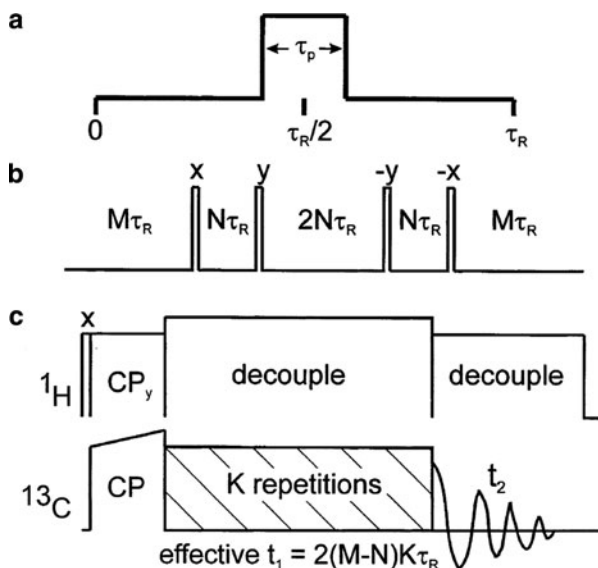


**Fig. 1** Pulse sequence for fpRFDR-CT measurements. (a) The fpRFDR sequence consists of a single  $\pi$  pulse of length  $\tau_p$  centered in each MAS rotation period  $\tau_R$ . (b) The fpRFDR sequence is incorporated into a multiple pulse cycle based on the WAHUHA cycle, by insertion of four  $\pi/2$  pulses with the indicated phases. Homonuclear dipole–dipole couplings generated by fpRFDR are scaled by a factor of  $(M - N)/(M + 2N)$ . (c) In the full 2D technique,  $^{13}\text{C}$  magnetization created by CP evolves under  $^{13}\text{C}$ – $^{13}\text{C}$  dipole–dipole couplings for an effective  $t_1$  period  $2(M - N)K\tau_R$  is kept constant.  $^1\text{H}$ – $^{13}\text{C}$  couplings are removed by proton decoupling fields during  $t_1$  and  $t_2$ . (Figures and caption adapted from [41]. Copyright (2001), with permission from Elsevier)

increase the nearest distance between two labeled  $\text{C}^\beta$  atoms to ca. 7 Å, for which there will be no significant signal dephasing observed in the fpRFDR-CT experiment. To quantify the spacing between the neighboring  $\beta$ -strands ( $d$ ), the fpRFDR-CT data can be compared with simulations on a linear chain of six spins with  $d$  varied from 4 to 7 Å. To reduce the “edge effect” of a finite spin system, the initial density operator may include only the polarization of the central two spins, whereas the detection operator includes all six spins [45]. Furthermore, the contribution from the background signals must be corrected for to warrant a meaningful comparison between the experimental and simulation data (see below) [44]. However, if there are two  $\beta$ -sheets closely interdigitated, as in the case of steric zipper [20], the interpretation of the fpRFDR-CT data would be less straightforward [52]. Also, the fpRFDR-CT data of  $\text{C}^\alpha$  is difficult to analyze quantitatively because of its fast  $T_2$  relaxation.

### 2.3.1 Correction of Background Signals

To illustrate the procedure of background signal correction, let us consider a hypothetical fibril system formed by polypeptides containing 21 residues, where a

chosen residue is  $^{13}\text{C}$  labeled at the carbonyl site. Assuming that 100% of the molecules are fibrillized and that the natural abundance signals do not dephase at all, the uncorrected  $C'$  fpRFDR-CT data can be written as

$$\frac{S_{\text{raw}}(\tau)}{S_{\text{raw}}(0)} = \frac{S^{\text{l,f}}(\tau) + S^{\text{na,u}}}{S^{\text{l,f}}(0) + S^{\text{na,u}}}, \quad (1)$$

where  $\tau$  denotes the effective dipolar dephasing time, and  $S^{\text{l,f}}$  and  $S^{\text{na,u}}$  indicate the signals arising from the labeled sites in fibrillar state and the sites of natural abundance (undephased), respectively. Accordingly, the  $C'$  fpRFDR-CT data are corrected as

$$\frac{S^{\text{l,f}}(\tau)}{S^{\text{l,f}}(0)} = \frac{S_{\text{raw}}(\tau) - S_{\text{raw}}(0) \times \frac{20 \times 1.1\%}{(1+20 \times 1.1\%)}}{S_{\text{raw}}(0) \times \left(1 - \frac{20 \times 1.1\%}{(1+20 \times 1.1\%)}\right)}. \quad (2)$$

In a more general case, some signals from natural abundance  $^{13}\text{C}$  nuclei will dephase ( $S^{\text{na,d}}$ ) because of the finite probability that they are in close proximity of other  $^{13}\text{C}$  nuclei. Furthermore, some labeled peptide molecules are unfibrillized and we assume that their signals will not dephase ( $S^{\text{l,u}}$ ). Consequently, we can write

$$\frac{S_{\text{raw}}(\tau)}{S_{\text{raw}}(0)} = \frac{S^{\text{l,f}}(\tau) + S^{\text{l,u}} + S^{\text{na,d}}(\tau) + S^{\text{na,u}}}{S^{\text{l,f}}(0) + S^{\text{l,u}} + S^{\text{na,d}}(0) + S^{\text{na,u}}}. \quad (3)$$

An estimation of the  $S^{\text{na,d}}$  signal can be obtained by measurements of the unlabeled fibril sample. For convenience, here we assume that 10% of the natural abundance signal will dephase, i.e.,  $S^{\text{na,d}} = S^{\text{na,u}} \times 0.1/0.9$ , so that we can write

$$\frac{\left(\frac{0.1}{0.9} + 1\right)S^{\text{na,u}}}{S_{\text{raw}}(0)} = \frac{20 \times 1.1\%}{1 + 20 \times 1.1\%}. \quad (4)$$

Similarly, we can obtain

$$\frac{\left(\frac{1-x_u}{x_u} + 1\right)S^{\text{l,u}}}{S_{\text{raw}}(0)} = \frac{1}{1 + 20 \times 1.1\%}, \quad (5)$$

where the factor  $x_u$  denotes the fraction of the unfibrillized samples. For a sufficiently long dephasing time (ca. 70 ms), the fraction of the residual  $^{13}\text{C}$  signal that does not decay to zero becomes

$$\frac{S_{\text{residual}}}{S_{\text{raw}}(0)} = \frac{S^{\text{l,u}} + S^{\text{na,u}}}{S_{\text{raw}}(0)}. \quad (6)$$

On the basis of (4)–(6) we can estimate  $x_u$  experimentally:

$$x_u = \frac{1}{0.82} \left( \frac{S_{\text{residual}}}{S_{\text{raw}}(0)} - 0.18 \times 0.9 \right). \quad (7)$$

Consequently, the signal fractions of  $S^{\text{l.f}}(\tau)/S^{\text{l.f}}(0)$  can be calculated and compared with simulations. For samples prepared by bacterial expression, correction of the background signals can be carried out in a similar fashion [48, 53, 54]. It is noteworthy that spin geometries deviated from linearity, which may occur in the side-chain  $^{13}\text{C}$  nuclei such as  $\text{C}^\beta$ , would produce more rapid signal decays and smaller residual signal fraction [55].

### 2.3.2 Torsion Angle Determination

The backbone torsion  $\phi$  angle is defined as the dihedral angle of  $\text{C}'_{(i-1)}\text{N}_{(i)}\text{C}^\alpha_{(i)}\text{C}'_{(i)}$ . Therefore, the  $\phi$  angle of the residue  $i$  can be determined by measuring the distance between  $\text{C}'_{(i-1)}$  and  $\text{C}'_{(i)}$  [56] and the most sensitive region of  $|\phi|$  is from 40 to 140° [57]. This strategy, together with other techniques based on tensor correlations (Sect. 6), has been applied to characterize the secondary structure of the bend region of  $\text{A}\beta_{1-40}$  fibrils [57]. In a similar fashion, the backbone torsion  $\psi$  angle of the residue  $i$ , which is defined as the dihedral angle of  $\text{N}_{(i)}\text{C}^\alpha_{(i)}\text{C}'_{(i)}\text{N}_{(i+1)}$ , can be determined by measuring the distance between  $\text{N}_{(i)}$  and  $\text{N}_{(i+1)}$ . Not surprisingly, the most sensitive region for  $|\psi|$  determination is quite comparable to that of  $|\phi|$  [47, 55]. For the measurements of multiple  $\text{N}_{(i)}\text{--}\text{N}_{(i+1)}$  distances, one could exploit the idea of  $\text{C}^\alpha$ -detection or the resolution enhancement provided by the  $\text{C}'\text{--}\text{C}^\alpha$  and  $\text{C}^\alpha\text{--}\text{C}^\beta$  correlations [55]. For the fibril samples formed by islet amyloid polypeptides, the  $\psi$  angle of the residue Phe23 extracted from the  $\text{C}^\alpha$ -detected  $^{15}\text{N}$  fpRFDR-CT data is consistent with a bend structure in the region of residues 18–27 [47].

### 2.3.3 PITHIRDS-CT

Although fpRFDR-CT is a constant-time technique, the effect of  $T_2$  relaxation is different as the positions of the WAHUHA pulses vary. Furthermore, a strong rf field is required to achieve the hard pulse approximation for WAHUHA, which could present a stringent condition for proton decoupling. As an alternative to the use of WAHUHA pulses, Tycko has developed a new approach to construct the constant-time version of fpRFDR [55]. In general, the cyclic time displacement of an arbitrary recoupling sequence by  $\tau_n$  will introduce a phase factor  $\exp(im\omega_r\tau_n)$  and will rotate the average Hamiltonian as follow [55]:

$$\bar{H}_n = e^{im\omega_r\tau_n} \left\{ U_{\text{rf}}(M\tau_r - \tau_n, 0) \bar{H} U_{\text{rf}}^\dagger(M\tau_r - \tau_n, 0)^{-1} \right\}, \quad (8)$$



where  $M\tau_r$  denotes the cycle time of the sequence and  $U_{\text{rf}}$  is the unitary operator defined by the rf field. We now consider the pulse sequence of fpRFDR and set  $\tau_n = 2\pi n/3\omega_R$ , where  $n = 0, 1, 2$ . Because each of the  $\pi$  pulses in fpRFDR has a duration of one-third of the rotor period, it can be shown that the corresponding operator of  $U_{\text{rf}}(M\tau_r - \tau_n, 0)$  is a unity operator. Consequently, if we concatenate  $\bar{H}_0$ ,  $\bar{H}_1$ , and  $\bar{H}_2$ , we will have

$$\bar{H}_0 + \bar{H}_1 + \bar{H}_2 = \{1 + e^{im\omega_r\tau_1} + e^{im\omega_r\tau_2}\}\bar{H} = 0. \quad (9)$$

The novelty of (9) is that the net homonuclear dipolar dephasing can be controlled by a systematic variation of the number of the  $\bar{H}_0$ ,  $\bar{H}_1$ , and  $\bar{H}_2$  blocks. This technique has the acronym of PITHIRDS-CT [55] and has the virtues that the effect of  $T_2$  is identical for all data points and that the rf field of all the pulses is only 1.67 times the spinning frequency. The only experimental concern is that very stable spinning or active rotor synchronization may be required for the implementation of PITHIRDS-CT.

## 2.4 Multiple-Quantum NMR

As discussed above, dipolar dephasing experiments can provide very valuable structural information for the study of amyloid fibrils. However, for a given dephasing rate, it is not trivial to deduce the number of spins constituting the spin cluster. In this regard, multiple-quantum (MQ) NMR is a powerful technique for spin counting because the observation of an  $n$ -quantum signal implies that there must be at least  $n$  spins coupled in a spin network [58]. The first application of MQ NMR to the study of amyloid fibrils was carried out under static condition [59]. With an excitation time of 14.4 ms, signals up to 5Q were observed for two singly labeled  $A\beta_{1-40}$  fibril samples ( $\text{Ala21-}^{13}\text{C}^\beta$  and  $\text{Ala30-}^{13}\text{C}^\beta$ ). These observations have firmly established that the  $\beta$ -sheet structure of the  $A\beta_{1-40}$  fibrils is in-register parallel [59]. At a magnetic field of 9.4 T, the total experimental time for each sample (10–15 mg) is approximately 100 h, with a recycle delay of 1 s. In addition to the issue of poor sensitivity, MQ NMR measurements for  $C'$  under static condition are very inefficient because of the large CSA. To tackle these problems, Oyster and Tycko have incorporated the fpRFDR sequence into some MQ NMR techniques developed for static solids [60]. The design principle is quite similar to that of fpRFDR-CT. For a singly labeled  $A\beta_{1-40}$  fibril sample ( $\text{Val39-}^{13}\text{C}'$ ), signals up to 3Q were observed with an excitation time of 31.1 ms under a spinning frequency of 18.519 kHz. The total experimental time is ca. 28 h for 8 mg of the sample. Although the sensitivity has greatly improved under MAS condition, the downscaling of the effective Hamiltonian leads to a substantially longer excitation time. On the other hand, the intramolecular 3Q signal has been observed in a uniformly  $^{13}\text{C}$  labeled fibril sample with an excitation time of 1.2 ms [60].

This observation illustrates an interesting possibility of probing torsion angles by a controlled evolution of the intramolecular MQ signals, just as discussed by Levitt and co-workers [61].

## 2.5 Polarization Transfer Via Homonuclear J-Coupling

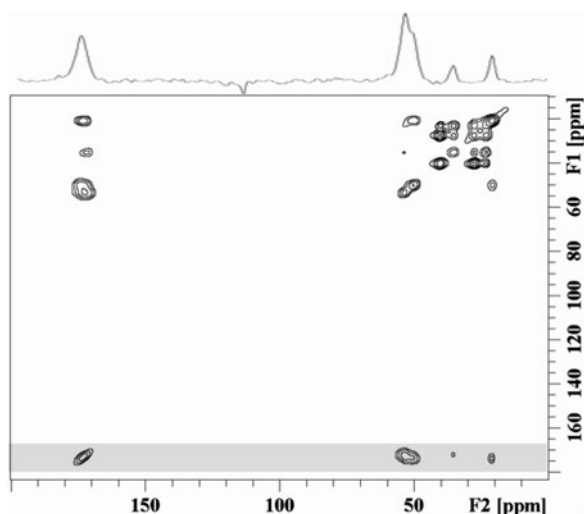
Under the high-resolution condition provided by MAS, it is possible to probe the correlations between different nuclei via the dipole–dipole interaction or the J-coupling [62, 63]. It is of great interest to pursue J-coupling mediated polarization transfer in SSNMR [64–76] both because of the selectivity offered by this through-bond interaction and because of the 100% theoretical transfer efficiency for a two-spin system. To realize polarization transfer via J-coupling, other internal interactions such as chemical shifts and homonuclear dipole–dipole coupling must be efficiently suppressed. A very successful pulse sequence for this purpose is total through-bond-correlation spectroscopy (TOBSY) [65]. A typical TOBSY sequence would create the following average Hamiltonian to the lowest order:

$$\bar{H} = 2\pi J_{\text{iso}} I \cdot S. \quad (10)$$

However, typical polarization transfer efficiency reported for  $^{13}\text{C}$ – $^{13}\text{C}$  TOBSY measurements of polypeptides is significantly less than the theoretical maximum. One of the major reasons is due to the requirement of high power  $^1\text{H}$  decoupling during the polarization transfer, which is usually set to be three times larger than the recoupling field [37, 77].

Many years ago, Yannoni et al. demonstrated that separate proton decoupling is in principle unnecessary for  $^{13}\text{C}$  nutation spectroscopy [78]. Recently, it has been shown in a  $^{13}\text{C}$  homonuclear dipolar recoupling experiment that MAS alone is sufficient for good  $^1\text{H}$  decoupling when the spinning frequency is high enough [38]. A systematic study has also shown that significant excitation of  $^{13}\text{C}$  homonuclear double-quantum coherence can be acquired without  $^1\text{H}$  decoupling [79]. This no-decoupling approach, coined as NO-DEC by Baldus and co-workers [79], was first tested for dipolar recoupling experiments. Intuitively, this NO-DEC approach can be immediately incorporated into most existing TOBSY-like sequences [65, 66, 70–73]. By numerical simulations we found that proton decoupling is indeed not necessary for the so-called R-TOBSY method, as long as the rf recoupling field is high enough. Experimentally, a good  $\text{C}' \rightarrow \text{C}^\alpha$  polarization transfer efficiency (>50%) in a uniformly labeled noncrystalline polypeptide has been achieved without  $^1\text{H}$  decoupling, for which the rf field was set to 125 kHz at a spinning frequency of 25 kHz [80] (Fig. 2). Although the chemical shift difference between  $\text{C}'$  and  $\text{C}^\alpha$  becomes larger at higher magnetic field, numerical simulations based on the R-TOBSY technique shows that the transfer efficiency at a field strength of 18.8 T is nearly identical to that at 7.05 T.

**Fig. 2**  $^{13}\text{C}$ – $^{13}\text{C}$  correlation spectrum measured for the MB(*i* + 4)EK polypeptides at 7.05 T under 25 kHz MAS spinning. The projection of the shaded region is shown to highlight the excellent  $\text{C}' \rightarrow \text{C}_\alpha$  transfer efficiency. (Figures and caption adapted from [80]. Copyright (2006), with permission from Elsevier)



## 2.6 Frequency-Selective Polarization Transfer

To achieve a more selective polarization transfer, e.g.,  $\text{C}' \leftrightarrow \text{C}^\alpha$ , the so-called multiple chemical shift precession (MCSP) could be employed to achieve frequency selective polarization transfer based on J-coupling [81]. The design principle of MCSP has a close analogy to the DANTE concept in the zero-quantum subspace. Consider the ZQ coherence excited by a TOBSY pulse block. Under free precession, the ZQ coherence will evolve at a frequency equal to the chemical shift difference ( $\Delta$ ) of the two interacting spins. As an analogy to the DANTE concept, a train of TOBSY pulse blocks can be used to excite selectively the desired ZQ coherence in a multiple-spin system, provided that the free precession period between two TOBSY blocks is set equal to the integer multiples of  $1/\Delta$ . That is, for other spin pairs whose chemical shift difference is different from  $\Delta$ , the flip-flop term of the average Hamiltonian will be truncated. Figure 3 shows the experimental results obtained for [U- $^{13}\text{C}$ ,  $^{15}\text{N}$ ]-alanine. The upper trace represents the regular TOBSY experiment, in which a significant portion of the  $\text{C}'$  polarization has been transferred to  $\text{C}^\alpha$  and  $\text{C}^\beta$ . As we set the precession period equal to  $1/\Delta$  and increase the  $N$  from 1 to 4, a significant increase in the  $\text{C}^\alpha$  polarization is produced at the expense of the  $\text{C}^\beta$  polarization. The selectivity of the MCSP approach depends on the number of precession periods. An optimum value for  $N$  has to be determined experimentally.

The idea of frequency selectivity is certainly not restricted to J-coupling mediated polarization transfer. Furthermore, frequency selective polarization transfer can also be realized by DQ recoupling techniques. For the technique of shift-evolution-assisted selective homonuclear recoupling (SEASHORE), which employs POST-C7 to construct an effective DQ coupling [82, 83], frequency selective polarization can be achieved when the transmitter offset is set to the

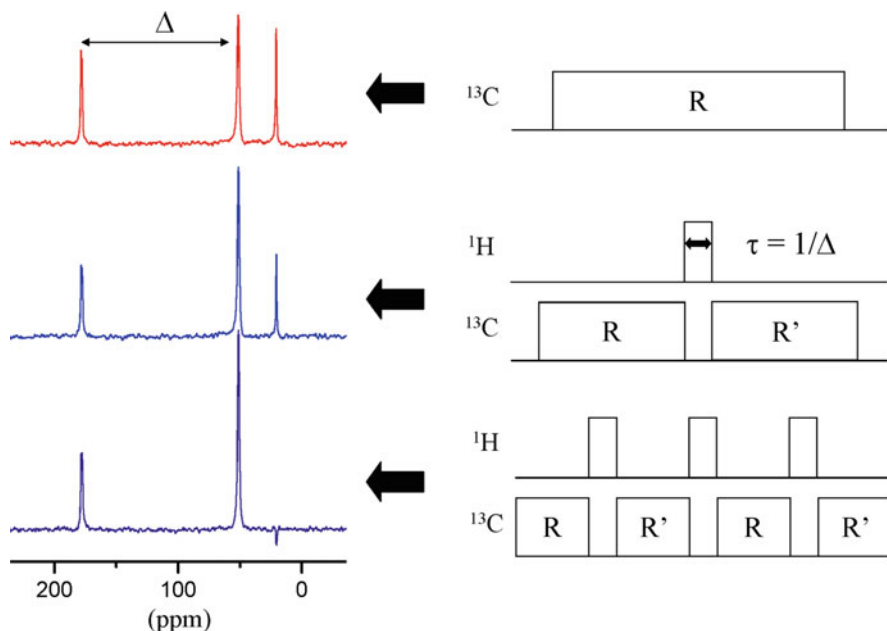


**Fig. 3** Experimental results measured for  $[U-^{13}\text{C}, ^{15}\text{N}]$ -alanine based on the MCSP approach. The polarization of  $\text{C}^\alpha$  after the mixing period increases as the number of R-TOBSY mixing periods increases to four. Accordingly, the  $\text{C}^\beta$  is nullified eventually. (Figure and caption adapted from [81]. Copyright (2006), with permission from Elsevier)

midpoint of the chemical shifts of the spin pair of interest, i.e.,  $(\omega_I + \omega_S) = 0$  [84]. In comparison, the frequency selectivity of MCSP depends on the duration of the free precession period, whereas SEASHORE may rely only on the transmitter position for its selectivity. The latter approach has the advantage that the free precession period can be set to multiples of the rotor period. Strictly speaking, the frequency selectivity is achieved in SEASHORE when the phase factor  $(\omega_I + \omega_S)n\tau_r$  is zero or a multiple of  $2\pi$ , where  $n\tau_r$  is the duration of the free precession period [84]. Very recently, the technique of fpRFDR has been incorporated in the framework of SEASHORE [85]. The resultant technique, viz. ZQ-SEASHORE, can achieve frequency selective dipolar recoupling under very fast MAS condition (40 kHz).

### 3 Heteronuclear Dipolar Recoupling Techniques

#### 3.1 REDOR

Rotational echo double resonance (REDOR) [86] is one of the most important techniques developed for solid-state NMR spectroscopy. The theory of REDOR is

well understood [87, 88] and requires no further discussion in this review. It has been shown that the distances along the peptide backbone obtained by  $^{13}\text{C}\{^{15}\text{N}\}$  REDOR measurements can provide useful constraints on the backbone torsion angles [89]. Another important application of REDOR in the studies of amyloid fibrils is the determination of the H-bond registry of the  $\beta$ -sheets. We will discuss some specific details relevant to this application in the following section.

To avoid the interference from intramolecular REDOR dephasing, peptides with  $^{15}\text{NH}_i$  labels could be mixed with peptides with  $^{13}\text{CO}_j$  labels in a 1:1 ratio before fibrillization, where  $i$  and  $j$  denote the residues with isotopic enhancement at the amide and carbonyl sites, respectively. If an in-register parallel  $\beta$ -sheet is considered as the hypothetical structure, the most adequate model for the analysis of the  $^{13}\text{C}\{^{15}\text{N}\}$  REDOR data measured for the case of  $i = j$  should be a  $^{15}\text{N}$ – $^{13}\text{C}$ – $^{15}\text{N}$  spin system, where the NCN angle is ca.  $127^\circ$  and the two  $^{15}\text{N}$ – $^{13}\text{C}$  distances are 5.3 and 5.5 Å (Fig. 4a). For the case of  $i = j + 1$ , the NCN angle should be  $154^\circ$  and the two  $^{15}\text{N}$ – $^{13}\text{C}$  distances 4.2 and 5.6 Å. Other combinations of  $i$  and  $j$  for an

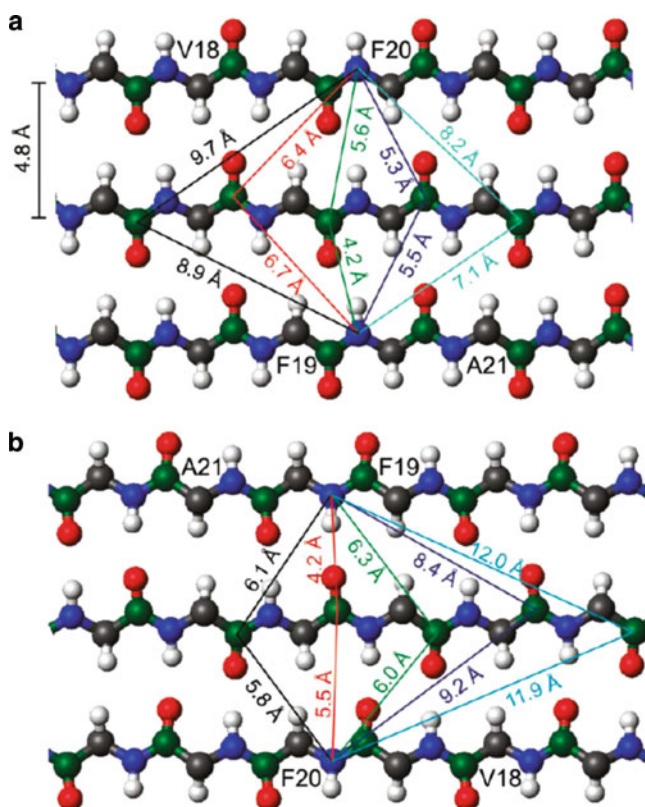


**Fig. 4** (a) Model for an in-register parallel  $\beta$ -sheet for REDOR simulations. Only the backbone is shown and the residue labels correspond to the sequence of  $\text{A}\beta_{1-40}$ . Relevant distances between Phe20 amide nitrogens (blue in color) and backbone carbonyl sites (dark green in color) are shown. (b) Model for an antiparallel  $\beta$ -sheet with  $17 + k \leftrightarrow 21 - k$  registry. (Figure and caption adapted from [51]. Copyright 2009 American Chemical Society)

in-register parallel  $\beta$ -sheet are not likely to produce any REDOR fraction ( $\Delta S/S_0$ ) larger than 0.1 [51]. For an antiparallel  $\beta$ -sheet (Fig. 4b), if the  $^{15}\text{NH}_i$  makes a hydrogen bond to the  $^{13}\text{CO}_j$  on a neighboring peptide chain, the REDOR dephasing can be analyzed based on the  $^{15}\text{N}$ – $^{13}\text{C}$ – $^{15}\text{N}$  spin system where the NCN angle is ca.  $180^\circ$  and the two  $^{15}\text{N}$ – $^{13}\text{C}$  distances are 4.2 and 5.5 Å. Furthermore, if the residues  $i$  and  $j$  are not hydrogen bonded, the corresponding REDOR fractions will be significantly smaller. Consequently, measurements of the  $^{13}\text{C}\{^{15}\text{N}\}$  REDOR data of the judiciously labeled samples can be carried out to determine the H-bond registry. Although the spin systems are based on idealized geometry, the agreement between the experimental and simulation data are usually quite satisfactory, provided that the contribution of the  $^{13}\text{C}$  signals arising from the unlabeled sites has been properly accounted for. A very detailed discussion of the procedure for background signal correction has been documented in the literature [44]. Because the  $^{13}\text{C}$ – $^{15}\text{N}$  distances targeting in our REDOR experiments are in the range of 4.5–5.5 Å, the required dephasing time is usually up to 50 ms. To minimize the  $T_2$  relaxation of the  $^{13}\text{C}'$  signals, we find that the REDOR pulse sequence developed by Anderson et al. [90], where the rotor synchronized  $\pi$  pulses are alternating between the dephasing and observe channels, is most suitable for the study of amyloid fibrils. Although a train of  $\pi$  pulses are applied in the  $^{13}\text{C}$  channel, the recoupling of  $^{13}\text{C}$  homonuclear dipole–dipole interaction should be negligible for the cross- $\beta$  motif because the closest  $^{13}\text{C}$ – $^{13}\text{C}$  distance within the same  $\beta$ -sheet layer is greater than 9 Å, provided that the peptides with  $^{15}\text{N}$  labels and those with  $^{13}\text{C}$  labels are well mixed before fibrillization. The situation is somewhat more complicated for those fibril samples formed by the polypeptides which contain the AGAAAAGA sequence. If this palindrome sequence is located in the core region of the fibrils, it is very likely that the two neighboring  $\beta$ -sheets would be closely packed to form the so-called steric zipper [20, 91]. As such, the interlayer distance could be as close as 5 Å [52]. In any case, one can monitor the attenuation of the reference signal ( $S_0$ ) as a function of the dephasing time to verify if there is any sizable homonuclear dipolar interaction among the  $^{13}\text{C}$  spins.

### 3.2 Frequency-Selective REDOR

Frequency-selective REDOR (fsREDOR) is a very powerful technique developed for the study of  $^{13}\text{C}$  and  $^{15}\text{N}$  uniformly labeled peptides or proteins [92]. The basic idea of this technique is to combine REDOR and soft  $\pi$  pulses to recouple a selected  $^{13}\text{C}$ – $^{15}\text{N}$  dipole–dipole interaction in a multiple-spin system. Usually one could use Gaussian shaped pulses to achieve the required selective  $\pi$  inversions. Other band selective shaped pulses have been developed for a more uniform excitation profile [93]. In its original implementation, fsREDOR was used to extract the internuclear distances of several model crystalline compounds [92]. In the past few years, this technique has proven to be very useful for the study of amyloid fibrils as well. For the Ure2p<sub>10–39</sub> fibril samples containing  $^{13}\text{C}$  and  $^{15}\text{N}$  uniformly

labeled Gln,  $^{13}\text{C}$  detected fsREDOR was used to assign the  $^{15}\text{N}$  signals arising from the side chain (111 ppm) and backbone amide sites (125 ppm), without measuring the more time-consuming  $^{13}\text{C}/^{15}\text{N}$  correlation spectrum. Experimentally, selective inversion of the  $^{15}\text{N}$  peak at 111 ppm produced greater dephasing of the Gln18  $\delta$ -carbon and selective inversion of the  $^{15}\text{N}$  NMR peak at 125 ppm produced greater dephasing of the  $^{13}\text{C}^\alpha$  signal [45]. For the WT A $\beta_{1-40}$  fibril samples with uniform  $^{15}\text{N}$  and  $^{13}\text{C}$  labeling at F20, D23, V24, K28, G29, A30, and I30, one can use fsREDOR to probe selectively the salt bridge resulting from the close proximity between D23 and K28 [51]. The viability of this method stems from the fact that the  $\text{C}_\gamma$  signal of D23 and  $\text{N}_\epsilon$  of K28 are well resolved from other backbone  $\text{C}'$  and amide  $^{15}\text{N}$  signals, respectively. In addition to these applications, fsREDOR has been incorporated in other newly developed techniques as discussed below.

### 3.3 DSQ-REDOR

Amyloid fibrils formed by peptides and proteins that are rich in glutamine or asparagine residues are of particular interest, both because of their involvement in neurodegenerative disorders such as Huntington's disease [94] and because of the hypothesis put forward by Perutz that these fibrils are stabilized by linear chains of hydrogen bonds among the side-chain amide groups of glutamine or asparagine. Perutz coined the phrase "polar zippers" to describe the putative side-chain hydrogen bonding interactions [95, 96]. However, it is not trivial to provide direct experimental evidence for the formation of polar zippers in amyloid fibrils. For each side chain the intraresidue  $^{15}\text{N}$ – $^{13}\text{C}$  dipole–dipole coupling amounts to 1,280 Hz, corresponding to a chemical bond distance of 1.338 Å [97]. If a linear chain of hydrogen bonds among the amide groups of glutamine is formed, the interresidue  $^{15}\text{N}$ – $^{13}\text{C}$  dipole–dipole coupling would be 25–78 Hz (3.4–5.0 Å nearest-neighbor  $^{15}\text{N}$ – $^{13}\text{C}$  distance). For  $^{13}\text{C}$  and  $^{15}\text{N}$  uniformly labeled samples, it is very difficult to characterize the relatively weak interresidue  $^{15}\text{N}$ – $^{13}\text{C}$  dipolar coupling in the presence of the strong intraresidue  $^{15}\text{N}$ – $^{13}\text{C}$  coupling by regular  $^{13}\text{C}\{^{15}\text{N}\}$  REDOR.

Very recently, a novel solid-state NMR technique has been developed by Tycko et al. to probe the formation of polar zippers in amyloid fibrils [45]. This technique is an extension of the fsREDOR techniques. Referring to Fig. 5, a short fsREDOR pulse train is applied during the pulse sequence period  $\tau_1$  to prepare intraresidue, heteronuclear "double single-quantum" (DSQ) coherences between directly-bonded  $^{13}\text{C}/^{15}\text{N}$  pairs in side-chain amide groups. DSQ coherences are represented by spin density operator terms of the form  $I_{1x}S_{1x}$  in the standard product operator formalism [100]. It is easy to show that the coherence  $I_{1x}S_{1x}$  is unaffected by the Hamiltonian of the form  $I_{1z}S_{1z}$ . In other words, the intraresidue DSQ coherences are unaffected by intraresidue  $^{15}\text{N}$ – $^{13}\text{C}$  couplings during the longer fsREDOR dephasing period  $\tau_d$ , but can decay due to intermolecular  $^{15}\text{N}$ – $^{13}\text{C}$  couplings pairs if such couplings are present. DSQ coherences at the end of  $\tau_d$  are converted to observable



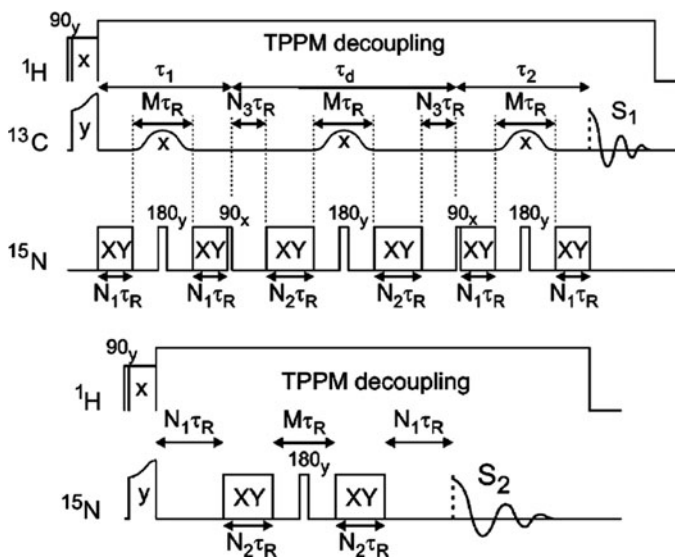


**Fig. 5** Radio frequency pulse sequences for measurements of  $S_1$  and  $S_2$  in DSQ-REDOR experiments. The MAS period  $\tau_R$  is 100  $\mu$ s. XY represents a train of  $^{15}\text{N}$   $\pi$  pulses with XY-16 phase patterns [98]. TPPM represents two-pulse phase modulation [99]. In these experiments,  $M = N_1 = 4$ ,  $N_2 + N_3 = 48$ , and  $N_2$  is incremented from 0 to 48 to produce effective dephasing times from 0 to 9.6 ms. Signals arising from intraresidue  $^{15}\text{N}$ - $^{13}\text{C}$  DSQ coherence ( $S_1$ ) are selected by standard phase cycling. Signal decay due to the pulse imperfection of  $^{15}\text{N}$  pulses is estimated by  $S_2$ . Decay due to the intermolecular  $^{15}\text{N}$ - $^{13}\text{C}$  dipole-dipole couplings is calculated as  $S_1(N_2)/S_2(N_2)$ . The phase cycling scheme can be found in the original figure and caption. (Figure and caption adapted from [45])

carbonyl  $^{13}\text{C}$  nuclear spin polarization by the final fsREDOR pulse train during period  $\tau_2$ .  $^{13}\text{C}$  NMR signals that arise from the DSQ coherences are selected by appropriate phase cycling of rf pulses in  $\tau_1$  and  $\tau_2$ . This technique has the acronym DSQ-REDOR. The DSQ-REDOR data obtained for the fibril sample formed by the fragment of Ure2p prion protein ( $^{13}\text{C}$  and  $^{15}\text{N}$  uniformly labeled at Gln18) are consistent with the structural motif of polar zipper [45]. In addition, DSQ-REDOR can also be used to determine the backbone  $\phi$  and  $\psi$  angles for peptide samples with uniform  $^{13}\text{C}$  and  $^{15}\text{N}$  labels at two consecutive residues [101]. The idea is to create the DSQ coherences for the  $^{13}\text{CO}_i$ - $^{15}\text{NH}_{i+1}$  pair. The excited DSQ coherences are then evolved under the influence of the dipolar interactions of the  $^{15}\text{NH}_i$ - $^{13}\text{CO}_i$  and  $^{15}\text{NH}_{i+1}$ - $^{13}\text{CO}_{i+1}$ . Thus, the dephasing of the DSQ coherence has an implicit dependence on the backbone torsion angles of  $\phi_{i+1}$  and  $\psi_i$ .

### 3.4 Band-Selective TEDOR

Another useful technique which is closely related to fsREDOR is the band-selective transferred echo double resonance (BASE TEDOR) [102]. As shown in Fig. 6, the



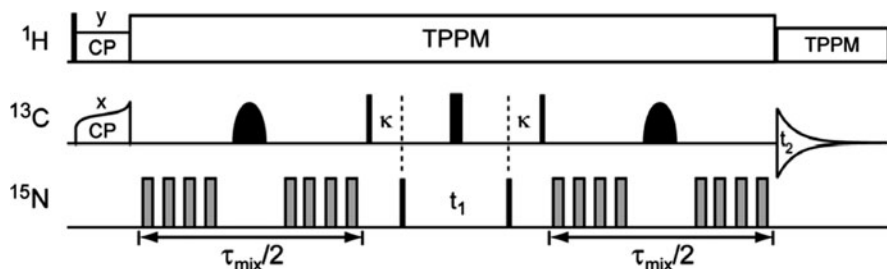


**Fig. 6** Pulse sequence of 3D band-selective TEDOR. The selective  $^{13}\text{C}$  pulses were applied in either the  $\text{C}^\alpha$  region ( $\sim 54$  ppm) or the  $\text{C}'$  region ( $\sim 174$  ppm). The short delays  $\kappa$  ensure that the total delay between the first and second REDOR periods is equal to an integer number of rotor cycles. For all sequences, the  $\pi/2$  and  $\pi$  pulses are represented by *thin* and *thick black rectangles*, respectively, and have phase  $x$ . The  $\pi$  REDOR pulses on the  $^{15}\text{N}$  channel (gray rectangles) were phase cycled according to the XY-4 scheme [98]. (Figure and caption adapted from the Supporting Information of [103]. Copyright 2010 American Chemical Society)

$^{13}\text{C}$  antiphase coherence generated in the first fsREDOR period is converted into the  $^{15}\text{N}$  antiphase coherence by a pair of  $\pi/2$  pulses on the  $^{15}\text{N}$  and  $^{13}\text{C}$  spins. With the middle band-selective  $\pi$  pulse applied in the  $\text{C}^\alpha$  (or  $\text{C}'$ ) region, the coherence transfer would occur between the amide nitrogen and  $\text{C}^\alpha$  (or  $\text{C}'$ ) only. In addition, the selective  $^{13}\text{C}$   $\pi$  pulse can refocus the J-couplings between the excited spins and other  $^{13}\text{C}$  spins which are outside the bandwidth of the selective pulse. After the chemical shift evolution in the  $^{15}\text{N}$  dimension ( $t_1$  evolution), the  $^{15}\text{N}$  antiphase coherence is then transferred back to the  $^{13}\text{C}$  antiphase coherence by the second fsREDOR period [102, 103]. As discussed in the foregoing section,  $^{15}\text{N}$  fpRFDR-CT or PITHIRDS-CT can be used to probe the backbone  $\psi$  angle when two consecutive amide sites are  $^{15}\text{N}$  labeled. However, the spectral resolution of the amide  $^{15}\text{N}$  is rather poor compared to that of  $\text{C}^\alpha$ . Therefore, one can employ the BASE TEDOR technique to transfer the  $^{15}\text{N}$  signals to the directly bonded  $\text{C}^\alpha$  for detection, when the samples are  $^{15}\text{N}$  and  $^{13}\text{C}$  uniformly labeled at multiple sites [55]. The  $^{13}\text{C}$ -detected  $^{15}\text{N}$  fpRFDR-CT data have been acquired for fibril samples formed by islet amyloid polypeptide, from which it has been shown that the Phe23 residue adopts a non- $\beta$ -strand conformation [47]. By a systematic variation of the fsREDOR period, the BASE TEDOR technique can be used to probe internuclear bond distances. In particular, the effective  $^{15}\text{N}$ – $^{13}\text{C}'$  and  $^{15}\text{N}$ – $^{13}\text{C}^\alpha$  one-bond dipolar couplings of selected residues of huPrP<sub>23–144</sub> fibrils were determined at a MAS frequency of 11.111 kHz. A variant of BASE TEDOR, known as z-filtered TEDOR, has also been employed to determine a few dozen of the one-bond and two bond C–N distances of the fibrils formed by the 11-residue fragment of human transthyretin [104].

### 3.5 $^1\text{H}$ – $X$ Dipolar Couplings

Any heteronuclear dipolar recoupling techniques developed for systems containing multiple  $^1\text{H}$  spins must have the property to suppress actively the  $^1\text{H}$ – $^1\text{H}$  dipolar

interaction. There are several methods to achieve this goal. In addition to the frequency-switched LG (FSLG) technique [105, 106], symmetry-based methods [107, 108] have also been developed for the characterization of C–H and N–H bond lengths. Site specific one-bond dipolar couplings of  $^{15}\text{N}$ – $^1\text{H}$  and  $^{13}\text{C}^\alpha$ – $^1\text{H}$  have been characterized for residues in the amyloid core region of huPrP<sub>23–144</sub> fibrils [103]. Together with the results of the effective  $^{15}\text{N}$ – $^{13}\text{C}'$  and  $^{15}\text{N}$ – $^{13}\text{C}^\alpha$  one-bond dipolar couplings, it has been deduced that the structural dynamics at the sub-microsecond time scale are approximately identical for residues located in different parts of the amyloid core [103]. Other applications of the recoupling techniques for  $^{15}\text{N}$ – $^1\text{H}^\text{N}$  and  $^{13}\text{C}^\alpha$ – $^1\text{H}^\alpha$  can be found in the tensor correlation methods for the measurements of backbone torsion angles (see Sect. 6).

## 4 Correlation Spectroscopy

Correlation spectroscopy is of paramount importance in solid-state NMR studies of biological solids. On the basis of the  $^{13}\text{C}$  and  $^{15}\text{N}$  chemical shifts, it is possible to estimate the backbone torsion angles if the secondary structure is in the  $\alpha$ -helix or  $\beta$ -sheet regions. This feature is particularly useful for the study of amyloid fibrils. Furthermore, the signal line widths can provide a reliable measure on the structural order. For well ordered fibrils, the line widths are usually in the region of 2–3 ppm for lyophilized samples, whereas the line widths would become 0.5–1.5 ppm for hydrated samples. Although one could rely on multidimensional techniques to enhance spectral resolution, very often one can also reduce the ambiguities in data analyses by comparing spectra obtained for the samples prepared with different labeling schemes. For example, by comparing the spectra of uniformly labeled samples with those of “diluted” samples (mixture of labeled and unlabeled samples), one can distinguish the distant constraints arising from intra- or intermolecular contacts. In this section, we will discuss some correlation techniques which have been successfully applied to the studies of amyloid fibrils.

### 4.1 Spectral Assignment

The  $^{13}\text{C}$  signals within a uniformly labeled residue can be assigned by broadband  $^{13}\text{C}$  homonuclear correlation spectroscopy. NMR techniques commonly employed for the spectral assignments of fibril samples include proton-driven spin diffusion (PDSD) [109], RFDR [36, 37], fpRFDR [38], dipolar assisted rotational resonance/ rf assisted diffusion (DARR/RAD) [110–112], dipolar recoupling enhanced by amplitude modulation (DREAM) [113], and TOBSY [65, 71, 73, 114]. It should be noted that there does not exist a universal technique optimized for all kinds of samples. The choice of technique largely depends on the peptide sequence, the isotopic labeling scheme, the desired measurement temperature, the inherent signal

line width, the static field strength, and the accessibility of the desired probe head. Below we will discuss some illustrative examples taken from the literature of amyloid fibrils.

The simplest techniques for  $^{13}\text{C}$  homonuclear correlation spectroscopy are the PDS and DARR, for which the polarization-transfer mechanism is illustrated in Fig. 7. The MAS frequency for PDS is usually adjusted to be smaller than one half of the chemical shift difference between the carbonyl and aliphatic regions, and the mixing time is in the range of 20–50 ms [115–117]. For DARR, the MAS frequency is adjusted in such a way that the carbonyl and aliphatic signals are close to but not exactly on rotational resonance, and the mixing time is in the range of 5–20 ms [19, 118], depending on whether cross peaks due to multiple-bond connectivity are desired. Both techniques have been applied to the study of amyloid fibrils in high field ( $\geq 14.1$  T). Because the MAS frequency is relatively low (ca. 10 kHz), a stable spinning can be maintained at relatively low temperature [119]. Other techniques listed above such as fpRFDR require the rf irradiation in the  $^{13}\text{C}$  channel and they have much higher efficiency for one-bond polarization transfer than PDS and DARR. The mixing time is usually in the range of 2–3 ms. The technique of fpRFDR is a viable option for the study of amyloid fibrils formed by relatively

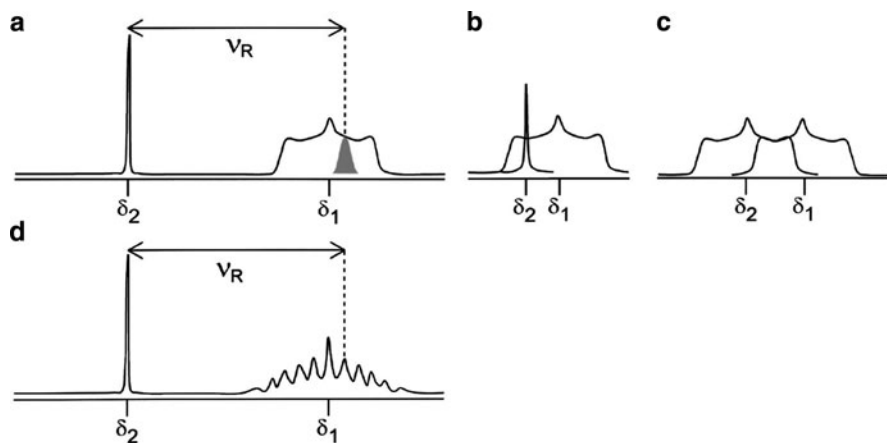


**Fig. 7** Schematic  $^{13}\text{C}$  MAS spectra of two  $^{13}\text{C}$  spins under  $^{13}\text{C}$ – $^1\text{H}$  recoupling, showing various types of spectral overlap necessary for energy conservation in  $^{13}\text{C}$ – $^{13}\text{C}$  polarization transfer. Spectrum (a) represents two resonances of  $\text{C}^{\text{ali}}$  at  $\delta_1$  and  $\text{C}'$  at  $\delta_2$ , where  $\text{C}^{\text{ali}}$  denotes any methine, methylene, and methyl carbons. The *hatched peak* denotes one of the spinning sidebands of the  $\text{C}'$  peak, being overlapped with the recovered  $^{13}\text{C}$ – $^1\text{H}$  dipolar powder pattern of the  $\text{C}^{\text{ali}}$  resonance. Spectrum (b) shows spectral overlap for a pair of spins whose chemical shift difference is smaller than the  $^{13}\text{C}$ – $^1\text{H}$  dipolar broadening. Spectrum (c) shows the case when spectral overlap occurs between two  $^{13}\text{C}$ – $^1\text{H}$  dipolar powder patterns. Spectrum (d) is similar to (a), but the  $^{13}\text{CH}$  resonance shows a sideband pattern induced by modulation of the  $^{13}\text{C}$ – $^1\text{H}$  dipolar interaction under suitable  $^1\text{H}$  rf irradiation. Spectral overlap is achieved for one of the spinning sidebands of the  $\text{C}'$  peak and one of the modulation-induced sidebands of the  $\text{C}^{\text{ali}}$  resonance. The *vertical dotted lines* denote the position of the spinning sideband of the  $\text{C}'$  peak. (Figure and caption adapted from [111]. Copyright [2003], American Institute of Physics)

short peptide sequence or full-length protein [54, 120], where the spinning frequency is usually in the range of 18–22 kHz. The DREAM technique is highly optimized for probing connectivity of the carbon signals in the aliphatic region under fast MAS frequency (25 kHz), whereas the transfer between  $C'$  and  $C^\alpha$  can also be realized under very fast MAS (40 kHz at a static field of 14.1 T) [121]. An interesting feature of the RFDR approach is that it could be applied without proton decoupling if the  $^{13}\text{C}$  recoupling field is around 120 kHz under fast spinning conditions [122]. Another NO-DEC technique developed for high-field and fast spinning conditions is cosine modulated adiabatic recoupling (CMAR) [123]. Both techniques have been applied to the study of amyloid fibrils [124, 125].

Recently, the use of paramagnetic relaxation enhancement (PRE) in biological solid-state NMR has received considerable attention [126–128]. On the basis of PRE, Ishii et al. have developed a very efficient strategy to carry out the  $^{13}\text{C}$  homonuclear correlation experiments (paramagnetic relaxation-assisted condensed data collection, PACC), for which convincing results have been obtained for amyloid fibrils [129]. In the presence of paramagnetic species (e.g., Cu-EDTA), the proton  $T_1$  relaxation of the  $\text{A}\beta_{1-40}$  and  $\text{A}\beta_{1-42}$  fibril samples can be shortened substantially. Under the condition of 40 kHz MAS, a very weak  $^1\text{H}$  decoupling (7 kHz, TPPM) is sufficient to provide a decent spectral resolution. Overall, the experimental recycle delay for PACC can be cut down to 0.2 s, rendering the measurements of fibril samples at the nanomole scale possible at 9.4 T. We note in passing that the effect of PRE on the  $^{13}\text{C}$  CPMAS spectra has also been used to probe the solvent exposed regions of  $\text{PrP}_{106-126}$  fibrils and oligomers [130].

For fibril samples comprising relatively short peptides prepared by solid-phase synthesis, the  $^{13}\text{C}$ – $^{13}\text{C}$  correlation spectra alone could provide site-specific  $^{13}\text{C}$  chemical shifts because the sequence positions of the labeled residues are known. However, for samples prepared by bacterial expression, techniques such as NCOCA and NCACX are required to carry out sequential assignment [121]. The coherence transfer between  $^{15}\text{N}$  and  $^{13}\text{C}$  nuclei is the basic step for sequential assignment techniques. There are two transfer mechanisms developed for the  $^{13}\text{C}$ – $^{15}\text{N}$  coherence transfer. For the technique of SPECIFIC CP, the  $^{13}\text{C}$  spin locking field is adjusted to be comparable to the resonance offset so that the matching of the Hartmann–Hahn conditions would depend on the position of the  $^{13}\text{C}$  transmitter [131]. As an illustration, the coherence transfer from  $^{15}\text{N}$  to  $C^\alpha$  and  $^{15}\text{N}$  to  $C'$  can be selected by placing the  $^{13}\text{C}$  transmitter at ca. 44 and 162 ppm, respectively, when the  $^{13}\text{C}$  and  $^{15}\text{N}$  rf fields are set to 5 and 30 kHz, respectively, under a MAS frequency of 25 kHz [121]. Alternatively, using the technique of BASE TEDOR or ZF-TEDOR, frequency selective  $^{13}\text{C}$ – $^{15}\text{N}$  coherence transfer can also be achieved [125, 132]. As shown in a study of  $\text{A}\beta_{1-40}$  fibrils, an evolution period of 2.87 ms could result in strong intraresidue  $^{13}\text{C}^\alpha$ – $^{15}\text{N}$  cross-peaks [132]. On the other hand, a mixing period of 6 ms is optimized for two-bond  $^{15}\text{N}_{(i+1)}$ – $^{13}\text{C}_{(i)}$  transfer, which can facilitate sequential assignment of the backbone signals [124].

The aforementioned assignment techniques based on dipole–dipole interactions are sufficient for the fibril samples with limited structural dynamics. In the presence of substantial dynamics, which may significantly attenuate the dipole–dipole

interactions between neighboring nuclei, the  $^{13}\text{C}\{^1\text{H}\}$  CP signals of some residues may become missing in the dipolar-based correlation spectra. As discussed earlier, the homonuclear polarization transfer of TOBSY proceeds through chemical bonds. Consequently, the TOBSY sequences have the same selectivity towards both the mobile and rigid parts of the system. This feature is an advantage in the study of hydrated fibril samples formed by sizable proteins or polypeptides. Using INEPT or CP as the preparation step for the subsequent TOBSY polarization transfer, one can select the  $^{13}\text{C}$  signals corresponding to either the mobile or the rigid parts, respectively [133]. The latter are usually originated from the core region of the amyloid fibrils [115, 134–136] and the mobile region is presumably solvent exposed [125]. To detect the signal arising from the mobile region of fibrils and to alleviate the interference of the signals from monomers, one can incorporate a  $T_2$  filter before the  $^{13}\text{C}\{^1\text{H}\}$  CP step as shown in Fig. 8 [5, 134].

It is well known that the fibrils formed by different fragments of the  $\beta$ -amyloid peptide could have different molecular structures [4]. While the studies of the fibril structures formed by a variety of protein fragments can deepen our understanding of the underlying biophysical principles of protein folding and misfolding, the fibrils formed by bona fide proteins remain to be the most biologically relevant targets. Very often, these targets such as prion protein have to be prepared by bacterial expression. Although the carbon sources of 1,3- $^{13}\text{C}$ -glycerol and 2- $^{13}\text{C}$ -glycerol could be used to enhance the spectral resolution, signal overlap may remain a severe problem when the molecular mass of the fibril-forming monomer becomes too large. In particular, when the number of cross-peaks is considerably smaller than the number of residues in the protein sequence, manual sequential assignment may become very difficult. Furthermore, it is important to check for the existence of any alternative sets of assignments which are consistent with the same set of spectra. To tackle this problem, Tycko et al. have developed a computer protocol based on a

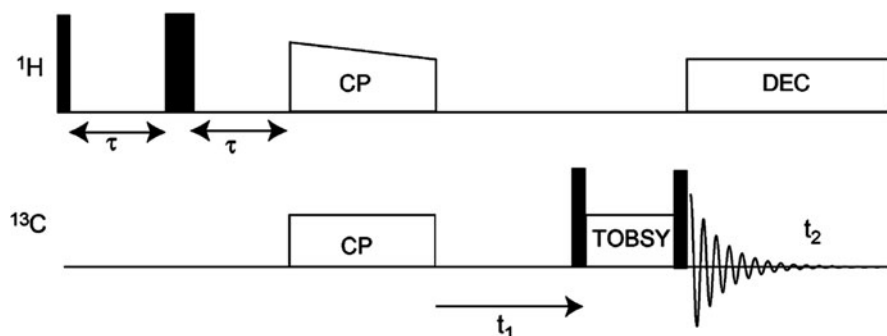


**Fig. 8** Pulse sequence for the measurement of homonuclear correlation spectra with  $T_2$  filtering. *Narrows bars* indicate  $\pi/2$  pulses and *broad bars* indicate  $\pi$  pulses. Experimental conditions employed for  $\alpha$ -synuclein fibrils samples: static field strength 9.4 T; temperature  $-5^\circ\text{C}$ ; spinning frequency 8 kHz;  $T_2$  filter 100 ms; CP contact time 2.5 ms; TOBSY mixing time 6 ms. The rf phases can be found in the original figure and caption. (Figure and caption adapted from the Supporting Information of [134]. Copyright (2005) National Academy of Sciences, USA)

Monte Carlo/simulated annealing (MC/SA) algorithm for sequential assignment in uniformly  $^{13}\text{C}$ ,  $^{15}\text{N}$ -labeled proteins [137]. The two-dimensional (2D) NCACX and NCOCX spectra measured for the fibril samples of full-length Syrian hamster prion protein (residues 23–231) have been analyzed by the MC/SA protocol, from which it has been concluded that the fibril core is formed primarily in the region of residues 173–224 [54].

## 4.2 Distance Constraints

When site specific  $^{13}\text{C}$  and  $^{15}\text{N}$  chemical shifts are available, preliminary structural conformation of the individual polypeptide strand can be obtained by TALOS calculations [138, 139], from which one can easily identify the  $\beta$ -sheet regions of the protein sequence. To refine the backbone conformation, one can use the proton-mediated techniques [140], viz. NHHc and CHHC, to probe the short-range  $\text{H}^{\text{N}}\text{--}\text{H}^{\alpha}$  and  $\text{H}^{\alpha}\text{--}\text{H}^{\alpha}$  contacts ( $\leq 3 \text{ \AA}$ ). Consider the framework of the NHHc pulse sequence. After the initial  $^{15}\text{N}\{^1\text{H}\}$  CP, the polarizations of  $\text{H}^{\text{N}}$  are prepared by the  $^1\text{H}\{^{15}\text{N}\}$  CP with a contact time of ca. 150  $\mu\text{s}$ . Then, a very brief  $^1\text{H}\text{--}^1\text{H}$  spin diffusion period (ca. 200  $\mu\text{s}$ ) is used to allow the contacts of  $\text{H}^{\text{N}}\text{--}\text{H}^{\alpha}$ , if any. Finally, the  $\text{H}^{\alpha}$  polarizations are transferred to  $\text{C}^{\alpha}$  for detection by another brief  $^{13}\text{C}\{^1\text{H}\}$  CP (150  $\mu\text{s}$ ). The CHHC experiment can be carried out in a similar fashion. As discussed by Baldus et al. [141], the sequential  $\text{H}^{\text{N}}_{(i+1)}\text{--}\text{H}^{\alpha}_{(i)}$  distance is less than 2.6  $\text{\AA}$  for the  $\beta$ -sheet conformation, whereas the distance is about 3  $\text{\AA}$  for  $\alpha$ -helices. Therefore, NHHc spectra are very useful for the identification of the core regions of amyloid fibrils [49, 134]. For fibril systems with antiparallel  $\beta$ -sheet organization, the CHHC experiment is well suited to determine the H-bond registry because the nearest distance of the  $\text{H}^{\alpha}$ s between the aligned residues is ca. 2.1  $\text{\AA}$  [10]. Furthermore, for the fibrils formed by an equimolar mixture of  $^{13}\text{C}$  labeled and  $^{15}\text{N}$  labeled monomers, only intermolecular contacts will be observed in the NHHc spectrum [49]. Both intermolecular and nonsequential intramolecular contacts obtained by NHHc and CHHC experiments are very important for structural determination [49].

To determine long-range homonuclear distance constraints, the techniques of PDSD and DARR are most commonly employed. Indeed, the PDSD technique has been employed to derive distance constraints for the first protein structure determined by solid-state NMR at 17.6 T [142]. When the mixing time is in the range of 250–1,500 ms, long-range contacts up to ca. 6  $\text{\AA}$  become detectable in DARR or PDSD experiments [132]. In the DARR spectra measured for  $\text{A}\beta_{1-42}$  fibrils, the cross peaks corresponding to the side-chain contacts between Phe19 and Leu34 have been observed, whereas the contact between Phe19 and Gly38 is missing [143]. This observation shows that the mature  $\text{A}\beta_{1-42}$  fibrils have a similar  $\beta$ -turn- $\beta$  structure as  $\text{A}\beta_{1-40}$  fibrils, which is not consistent with a previous conclusion based on mutagenesis results [144]. Nonetheless, it is well known that a slight difference in incubation conditions can result in different molecular structures for amyloid fibrils [145]. From the DARR spectra of the samples prepared by a 1:1 mixture of

two differently labeled  $A\beta_{1-42}$  peptides, where one peptide was labeled at the  $^{13}\text{C}^{\delta}$ -Gln15 and the other at the  $^{13}\text{C}^{\alpha}$ -Gly37, the observation of the cross-peak between  $\text{C}^{\delta}$ -Gln15 and  $\text{C}^{\alpha}$ -Gly37 indicates that  $\beta$ -strand staggering occurs in  $A\beta_{1-42}$  fibrils [143], just as observed for  $A\beta_{1-40}$  fibrils [132]. Note that for a nonstaggered geometry, the predicted distance between the labeled sites would be longer than the detection limit of DARR.

The architecture of  $\beta$ -sheet is also very important in the determination of fibril structures. Given that the side chains of even-numbered and odd-numbered residues in the same  $\beta$ -sheet point in opposite directions, any side-chain contacts between odd-numbered and even-numbered residues observed in PDSO or DARR spectra may indicate bend structures or intersheet contacts. With this consideration, the quaternary contacts of the basic cross- $\beta$  units have been found to be different for two morphologically distinct  $A\beta_{1-40}$  fibrils [132, 146]. As another example, the quaternary contacts between  $\beta$ -sheets of the nonfibrillar oligomers formed by  $\text{PrP}_{106-126}$  are found to be similar to those in fibrillar state [130]. Very recently, it has been shown that the band selective RFDR (BASE RFDR), where selective  $\pi$  pulses are used in the RFDR recoupling pulse train, is significantly more efficient than DARR for probing long-range contacts [147]. Another useful technique for the measurement of long-range  $^{13}\text{C}$ - $^{13}\text{C}$  or  $^{15}\text{N}$ - $^{15}\text{N}$  distances is the proton assisted recoupling (PAR) technique [148]. The transfer mechanism of PAR is based on the higher order effect, for which the dipolar truncation effect [149] is largely attenuated. The PAR technique has been used to probe the intermolecular backbone contacts of GNNQQNY fibrils and the results are consistent with an in-register parallel alignment [25].

For the determination of heteronuclear long-range contacts, ZF-TEDOR with long mixing time is a promising approach [150]. This method has been used to study the fibrils formed by a 50:50 mixture of  $[^{15}\text{N}, ^{12}\text{C}]$ - and  $[^{14}\text{N}, ^{13}\text{C}]$ -labeled  $\beta_2$ -microglobulin monomers [151]. At a mixing time of 16 ms, a number of intermolecular  $^{13}\text{C}$ - $^{15}\text{N}$  distances in the range of 5–5.5 Å have been detected. The results prove that the fibrils adopt an in-register parallel  $\beta$ -sheet structure [151].

### 4.3 *H/D Exchange Detected by Correlation Spectroscopy*

We have shown that correlation spectroscopy is of great utility for spectral assignments and for measurement of distance constraints. Here, we show that the  $^{13}\text{C}$ - $^{15}\text{N}$  correlation spectroscopy can also be exploited to monitor hydrogen/deuterium (H/D) exchange experiments. H/D exchange can be used to identify solvent-protected backbone amide protons in amyloid fibrils [144, 152, 153]. In brief, the amyloid fibrils are first incubated in deuterated buffer. After quenching the H/D exchange, the fibrils must be disaggregated into monomers. The residues at which the amide protons are exchanged to deuterons can then be detected by mass spectrometry [154] or solution-state NMR spectroscopy [155]. The most challenging step is the rapid conversion of the fibrils into the corresponding

monomers for subsequent detection. Although *d*6-DMSO is a reliable solvent for the dissolution of amyloid fibrils, it is not trivial to minimize the effect of backward exchange [155]. Different solvent mixtures have been suggested for different amyloid systems, showing that it is largely an empirical task to prepare the quenching buffer for an H/D exchange experiment [156]. Recently, we find that the dissolution of the amyloid fibrils is not necessary when  $^{13}\text{C}$ – $^{15}\text{N}$  correlation spectroscopy is used as the detection method [50]. That is, the technique of  $^{15}\text{N}\{^1\text{H}\}$  CPMAS can be used to select the signals of the nitrogen atoms which are in close proximity to protons. In particular, when the CP contact time is set to 100  $\mu\text{s}$ , the  $^{15}\text{N}$  signals of the deuterated amide groups would be largely suppressed. By this simple strategy, the in situ characterization of H/D exchange in amyloid fibrils could be realized.

As a proof-of-principle experiment, we measured the  $^{15}\text{N}\{^1\text{H}\}$  CP spectra of the amyloid fibrils formed by huPrP<sub>127–147</sub> (Ac-GYMLGSAMSRPIIHFGSDYED-NH<sub>2</sub>), which is  $^{15}\text{N}$  and  $^{13}\text{C}$  labeled at P137 and S143. Figure 9 shows the spectra of the fibril sample (without any H/D exchange) obtained at two contact times, viz. 2 ms and 100  $\mu\text{s}$ . For the 2-ms spectrum, two amide nitrogen signals are observed, in which the peaks at 135 and 117 ppm are assigned to the amide nitrogen of P137 and S143, respectively [89]. When the CP contact time is reduced to 100  $\mu\text{s}$ , the  $^{15}\text{N}\{^1\text{H}\}$  CP signal would be dominated by the one-bond  $^1\text{H}$ – $^{15}\text{N}$  transfer, which is referred to as the  $^{15}\text{N}^{\text{H}}$  signal in the subsequent discussion. Accordingly, the  $^{15}\text{N}^{\text{H}}$  signal of P137 is not detectable because proline does not have any amide proton. As expected, the  $^{15}\text{N}^{\text{H}}$  signal of S143 is still observable under the same experimental condition, which has approximately the same intensity as the 2-ms  $^{15}\text{N}\{^1\text{H}\}$  signal. Therefore, it is plausible to monitor the H/D exchange of amide protons by measuring the corresponding  $^{15}\text{N}^{\text{H}}$  signals without disassembling the fibrils into monomers. We first define the protection factor of the amide proton as the ratio of the  $^{15}\text{N}^{\text{H}}$  signal intensities of the sample with and without H/D exchange. After

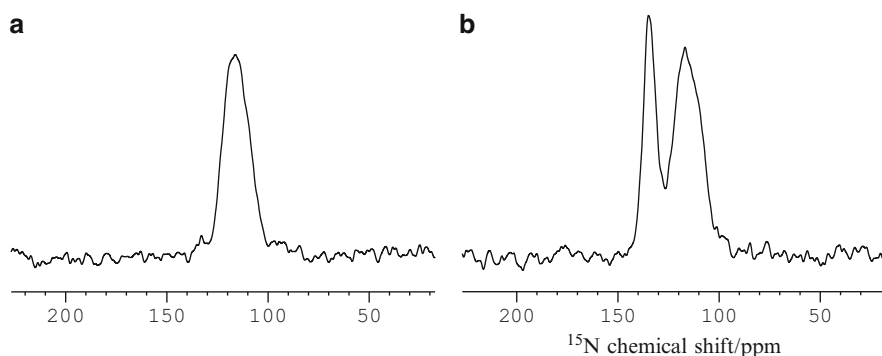


**Fig. 9**  $^{15}\text{N}\{^1\text{H}\}$  CPMAS spectra of the fibril sample formed by huPrP<sub>127–147</sub> ( $^{15}\text{N}$  labeled at P137 and S143) at a spinning frequency of 20 kHz. (a) Contact time of 100  $\mu\text{s}$ . (b) Contact time of 2 ms. (Figure and caption adapted from [50]. Copyright 2010 WILEY-VCH Verlag GmbH & Co. KGaA, Weinheim)



42-h H/D exchange, the protection factors were found to be  $0.07 \pm 0.03$  and  $0.6 \pm 0.3$  for S143 and I138, respectively. The relatively large errors are mainly due to the uncertainty of the amount of salts left in the samples. To alleviate this problem, we redefine the protection factor as the ratio of the signal intensities of  $^{15}\text{N}^{\text{H}}$  and  $^{15}\text{N}$ , where the contact time of the corresponding  $^{15}\text{N}\{^1\text{H}\}$  CP experiments were set to 100  $\mu\text{s}$  and 2 ms, respectively. The thus obtained protection factor for I138 is  $0.65 \pm 0.1$ . The error bar was determined by the root-mean-square noise of the spectrum. For measurements on uniformly labeled fibril samples, our strategy can be easily combined with 2D  $^{13}\text{C}\{^{15}\text{N}\}$  correlation spectroscopy [50].

## 5 Recoupling of Chemical Shift Anisotropy

Under MAS alone, anisotropic interactions such as CSA and dipole–dipole couplings are averaged to zero, provided that the spinning frequency is sufficiently high. Since anisotropic interactions usually have a direct or indirect dependence on molecular structure, numerous techniques have been developed to reintroduce these interactions under MAS. Various CSA recoupling techniques have been proposed and their merits have been briefly discussed by Schmidt-Rohr and co-workers [157]. Many of these CSA recoupling methods are not applicable to homonuclear dipole–dipole coupled systems or at MAS frequencies higher than 15 kHz, either because finite-pulse effects become dominant or because the required rf fields become too high to be practical. In this section, we describe the technique of recoupling of chemical shift anisotropy (ROCSA) [158]. The major advantages of ROCSA are: (1) that the effects of homonuclear dipole–dipole interactions are strongly suppressed; (2) that the lineshape of the recoupled CSA pattern is identical to the corresponding static powder pattern; (3) that the required rf field (in kHz) is only about four times the MAS frequency; (4) that only phase shifts in multiples of  $90^\circ$  are required.

### 5.1 Theory of ROCSA

Under MAS at frequency  $\omega_r = 2\pi\nu_r$ , the high-field Hamiltonian of a spin-1/2 system takes the following form in the rotating frame:

$$H(t) = H_{\text{rf}}(t) + H_{\text{int}}(t), \quad (11)$$

$$H_{\text{int}}(t) = \sum_{\Lambda m \lambda} \omega_m^\Lambda \exp(im\omega_r t) T_{\lambda 0}^\Lambda, \quad (12)$$

where  $\Lambda$  represents various internal interactions,  $\omega_m^\Lambda$  are the orientation-dependent coefficients of the Fourier components of the spatial functions ( $-2 \leq m \leq 2$ ), and

$T_{\lambda 0}^{\Lambda}$  are irreducible tensor operators of rank  $\lambda$ . The Hamiltonian of a static powder sample can be easily derived from the MAS Hamiltonian by setting  $\omega_r = 0$ :

$$H_{\text{int}} = \sum_{\Lambda m \lambda} \omega_m^{\Lambda} T_{\lambda 0}^{\Lambda}. \quad (13)$$

ROCSA makes use of the  $CN_n^v$  sequences [82, 159] to generate a static CSA powder pattern under MAS condition. The average Hamiltonian for a  $CN_n^v$  sequence is [159]

$$\begin{aligned} \bar{H}(t_q) &= \sum_{\Lambda L m \lambda \mu} (i)^{\mu} \omega_{Lm\lambda\mu}^{\Lambda} \exp(im\omega_r t_0) d_{\mu 0}^{\lambda}(-\beta_{rf}) \\ &\times \sum_q \exp\left(+iq \frac{2\pi}{N}(mn - \mu v)\right) T_{\lambda\mu}^{\Lambda}. \end{aligned} \quad (14)$$

All the symbols carry their usual meanings. If we want to create an average Hamiltonian similar to the static one, we just need to keep the terms associated with  $T_{20}^{CS}$ . Furthermore, the scaling factors of those terms should be identical. With the pulse sequence of  $Cn_n^1$  [160, 161], the symmetry allowed terms are ( $m = 0, \pm 1, \pm 2; \mu = 0$ ) for  $n \geq 3$ . For convenience we define the following scaling factors:

$$\chi_m^{\lambda} = \frac{1}{\tau_r} \int_0^{\tau_r} d_{00}^{\lambda}(-\beta_{rf}) \exp(im\omega_r t) dt. \quad (15)$$

We want to derive a specific subcycle for  $Cn_n^1$  such that the scaling factors  $\chi_m^{\lambda}$  are identical for  $m$  equal to  $\pm 1$  and  $\pm 2$ . In general, we have  $\chi_m^{\lambda} = (\chi_{-m}^{\lambda})^*$  and therefore the conditions  $\chi_m^{\lambda} = \chi_{-m}^{\lambda}$  are equivalent to the conditions that  $\chi_m^{\lambda}$  are real numbers. In particular, if we have a mirror symmetry of

$$\beta_{rf}(t) = \beta_{rf}(\tau_r - t), \quad (16)$$

for  $0 \leq t \leq \tau_r$ , we can obtain

$$\chi_m^{\lambda} = \frac{1}{\tau_r} \left\{ \int_0^{\tau_r/2} d_{00}^{\lambda}(-\beta_{rf}(t)) \exp(im\omega_r t) dt + \int_{\tau_r/2}^{\tau_r} d_{00}^{\lambda}(-\beta_{rf}(\tau_r - t')) \exp(im\omega_r t') dt' \right\}. \quad (17)$$

Setting  $\tau_r - t' = t$  for the second integral, we then have

$$\chi_m^\lambda = \frac{1}{\tau_r} \times \left\{ \int_0^{\tau_r/2} d_{00}^\lambda(-\beta_{\text{rf}}(t)) \exp(im\omega_r t) dt - \int_{\tau_r/2}^0 d_{00}^\lambda(-\beta_{\text{rf}}(t)) \exp(im\omega_r(\tau_r - t)) dt \right\}, \quad (18)$$

$$\chi_m^\lambda = \frac{2}{\tau_r} \left\{ \int_0^{\tau_r/2} d_{00}^\lambda(-\beta_{\text{rf}}(t)) \cos(m\omega_r t) dt \right\}. \quad (19)$$

Consequently, under the mirror symmetry described in (16),  $\chi_m^\lambda$  must be real because

$$d_{00}^\lambda(\beta) = \sum_{k=0}^{\lambda} (-1)^k \frac{(\lambda)!(\lambda)!}{(\lambda-k)!k!(\lambda-k)!(k)!} \left(\cos\frac{\beta}{2}\right)^{2(\lambda-k)} \left(\sin\frac{\beta}{2}\right)^{2k}, \quad (20)$$

where  $k$  is an integer.

Now consider the pulse sequence in Fig. 10. Each repetition of C spans one rotor period. Between 0 and  $\tau_r/2$ , the composite “ $0\pi$ ” pulse  $90_0 360_{180} 270_0$  is applied. This composite pulse, which has been commonly referred to as POST, is chosen because it has been shown to compensate for effects of rf inhomogeneity [83]. The mirror-image composite pulse is applied between  $\tau_r/2$  and  $\tau_r$ . With this particular design of ROCSA, the homonuclear dipole–dipole interaction is considerably suppressed relative to the CSA.

## 5.2 ROCSA Spectra of Amyloid Fibrils

It has been shown both theoretically and experimentally that  $C^\alpha$  CSA values are useful parameters to probe the local structures of biological systems [162, 163]. By comparison of the experimental CSA values with the calculated shielding surfaces, one may obtain an estimation of the backbone torsion angles of the corresponding residues. As an illustration, Fig. 11 shows the ROCSA spectra measured for the  $A\beta_{11-25}$  fibril sample which was uniformly  $^{13}\text{C}$ ,  $^{15}\text{N}$ -labeled at Val18 [158]. Isotropic  $^{13}\text{C}$  chemical shift data indicate that Val18, Phe19, Phe20, and Ala21 adopt  $\beta$ -strand conformations in  $A\beta_{11-25}$  fibrils. The  $C^\alpha$  CSA values obtained by ROCSA measurements are consistent with  $\beta$ -strand conformations at these residues. As illustrated in the studies of microcrystalline proteins, ROCSA can be used to obtain structural constraints on the secondary structure by characterizing the chemical shift tensors of the backbone carbons [163]. We expect that such an approach should also find fruitful applications in the study of amyloid fibrils.

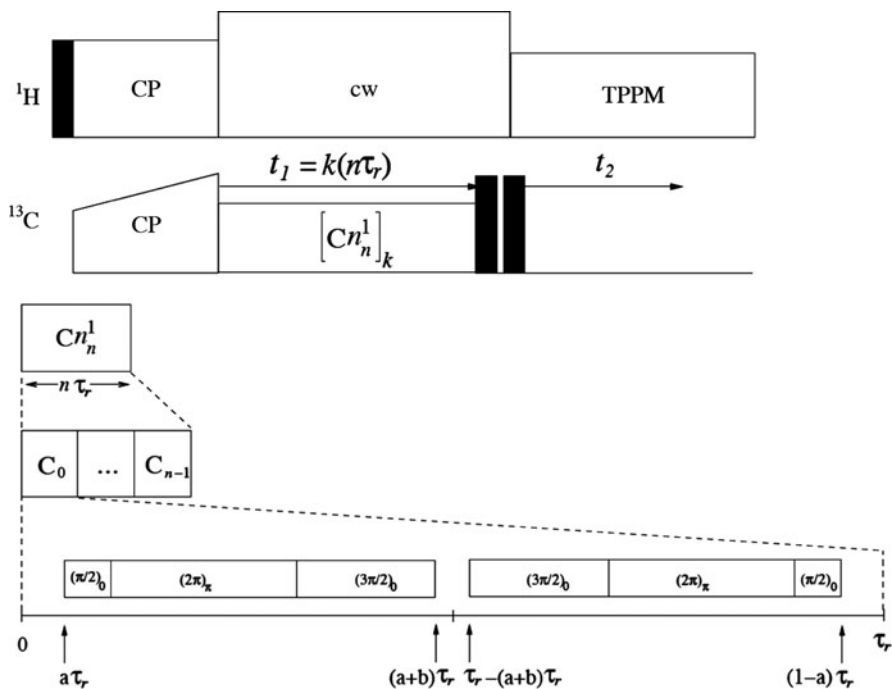


**Fig. 10** ROCSA pulse sequence based on  $Cn_n^1$  symmetry. The *rectangular blocks in black* represent  $\pi/2$  pulses. The recoupling period ( $t_1$ ) comprises  $k$  cycles of  $Cn_n^1$ . Each complete cycle of  $Cn_n^1$  spans  $n$  rotor periods ( $n\tau_r$ ). The rf phase of each  $C_q$  subcycle is set equal to  $2\pi q/n$ , where  $q$  is an index running from 0 to  $n - 1$ . Within each  $C_q$  subcycle,  $a\tau_r$  and  $b\tau_r$  indicate the position and the duration of the POST composite pulse, respectively. We find that the solution  $(a, b) = (0.0329, 0.467)$  is a favorable choice for the suppression of the homonuclear dipole–dipole interaction. The *bracketed and subscripted values* indicate the pulse length and rf phase in radians, respectively. (Figure and caption adapted from [158]. Copyright [2003], American Institute of Physics)

For polypeptides with inherent structural disorders, the  $^{13}\text{C}$  signals in the carbonyl region are usually poorly resolved. Therefore, the characterization of the  $C'$  CSA, which is sensitive to the  $\text{C} = \text{O} \cdots \text{HN}$  hydrogen bond strength, will become very difficult if more than one carbonyl carbon are  $^{13}\text{C}$  labeled. Because the  $C^\alpha$  signals of polypeptides are usually better resolved than the  $C'$  signals, one may transfer the  $C'$  CSA patterns to the neighboring  $C^\alpha$  for subsequent detection. This “ $C^\alpha$ -detection” scheme has been developed on the basis of ROCSA and R-TOBSY [164]. That is, the  $C'$  CSA is first recoupled by ROCSA and then the pattern is transferred to  $C^\alpha$  for detection by R-TOBSY. Dipolar-based polarization transfer techniques such as fpRFDR are not suitable in the present context because the  $C'-C^\alpha$  dipolar interaction will modulate the  $C'$  CSA pattern and such modulation may depend on the relative orientation of the  $C'$  and  $C^\alpha$  chemical shift tensors, which is usually unknown. Figure 12 shows the  $C^\alpha$ -detected  $C'$  CSA patterns of the amyloid fibrils formed by the peptide fragment of PrP<sub>109–122</sub>, in which the residues

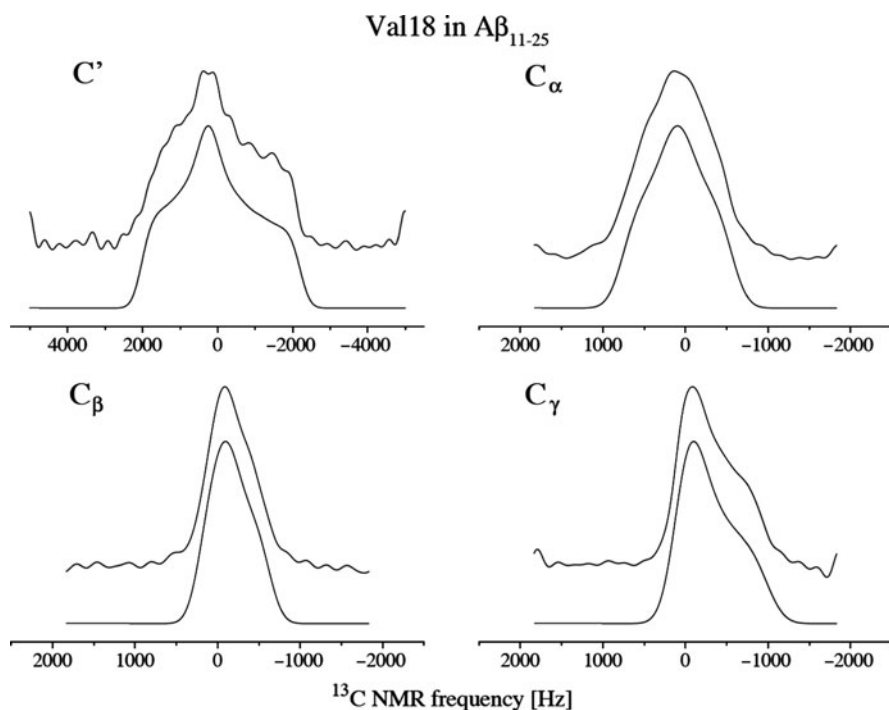


**Fig. 11** ROCSA spectra for Val-18 of  $A\beta_{11-25}$  fibrils. The  $C'$  spectrum was measured at 9.39 T under a MAS frequency of 20 kHz. The other spectra were measured at 14.09 T under the frequency of 11 kHz. *Upper traces* are experimental spectra. *Lower traces* are best-fit simulations for one-spin system. The rf carrier frequency is at 0 Hz. (Figure and caption adapted from [158]. Copyright [2003], American Institute of Physics)

Ala113, Gly119, and Val122 are uniformly  $^{13}\text{C}$ - and  $^{15}\text{N}$ -labeled [164]. The  $C'$  signals of Ala113 and Val122 are overlapping but their  $C^\alpha$  signals are well resolved. The minor distortion of the  $C'$  CSA pattern of Val122 may be attributed to the structural disorder at the C terminus of the polypeptide. Studies on other model compounds indicate that the  $C^\alpha$ -detection scheme for  $C'$  CSA pattern is a robust one, as long as the spin-lattice relaxation times of the  $C'$  and  $C^\alpha$  signals are significantly longer than the polarization transfer period. Again, the idea of  $C^\alpha$ -detection can be incorporated easily in existing homonuclear correlation techniques.

## 6 Tensor Correlation Methods

Tensor correlation methods refer to the selection of two anisotropic interactions so that the pattern of the 2D correlation spectrum can reveal the magnitudes and relative orientation of the two tensorial interactions. Below we will discuss many different SSNMR techniques suggested for the determination of peptide backbone

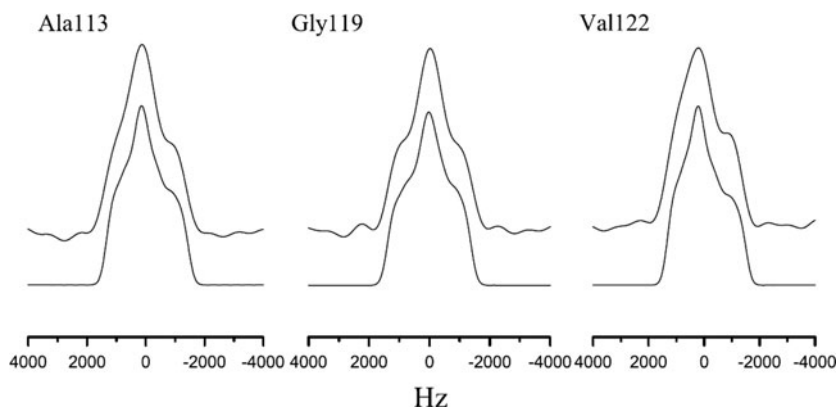


**Fig. 12**  $C_\alpha$ -detected  $C'$  CSA patterns of the SHPrP<sub>109–122</sub> fibril sample. The *upper* and *lower* traces correspond to the experimental and simulated spectra, respectively. Simulations correspond to the evolution of a one-spin system under the ROCSA sequence. The only variables are the chemical shift anisotropy and the asymmetry parameter. A Gaussian window function of 400 Hz was applied to the simulated spectrum before the Fourier transformation. (Figure and caption adapted from [164]. Copyright (2007), with permission from Elsevier)

torsion angles  $\phi$  and  $\psi$  under MAS. These techniques are all based on the principle of tensor correlation [165–167].

## 6.1 Backbone Phi–Psi Angle Determination

The correlation of the chemical shift tensors of two neighboring carbonyl carbons, say,  $C'_{(i)}$  and  $C'_{(i+1)}$ , can be exploited to determine the backbone torsion  $\phi$  and  $\psi$  angles of the residue  $i + 1$ . Because of the symmetry properties of the  $C'$  chemical shift tensor and the peptide plane, this approach cannot distinguish the conformations corresponding to  $(\phi, \psi)$  and  $(-\phi, -\psi)$  [168]. That is, a unique solution for  $(\phi, \psi)$  is not warranted in general, unless the alternative solution is not allowed sterically. The first technique which exploits this correlation approach is the 2D MAS exchange experiment [168, 169]. Other useful techniques include DQDRAW [56, 170] and DQCSA [171]. The utility of these methods relies on the assumption that the orientation of the  $C'$  chemical shift tensor with respect to the peptide plane is insensitive to the variation of the peptide conformation and the formation of hydrogen bonds. Theoretical calculations carried out for a model glycyl–glycine dipeptide at the DFT-IGLO level lend strong support to this basic assumption [172]. On the other hand, it has been shown by NMR measurements on model peptides that the most shielded principal component ( $\delta_{33}$ ) is always perpendicular to the peptide plane, whereas the orientation of the principal components lying in the peptide plane has a variation of about  $25^\circ$  [173–179]. A more comprehensive discussion of this issue can be found in a recent review [180]. Thus, the systematic

errors of the backbone torsion angles determined by the  $C'_{(i)}-C'_{(i+1)}$  approach are mainly due to the uncertainty in the tensor orientation of the  $C'$  carbon. Nonetheless, the intrinsic structural inhomogeneity commonly found in amyloid fibrils would presumably render this uncertainty immaterial. The major disadvantage of this method is that each labeled sample can allow the determination of one pair of  $\phi$  and  $\psi$  angles only.

For the study of  $A\beta_{1-40}$  fibrils, it is very important to characterize the conformation of the non- $\beta$ -sheet region (residues 25–29) in order to construct the molecular model for the fibrils. On the basis of the measurements of 2D MAS exchange and DQCSA, site specific torsion angles were obtained for the bend region of  $A\beta_{1-40}$  fibrils [57]. Because of the multiplicity in the sign choices for the obtained  $\phi$  and  $\psi$  angles, however, dimensional constraints obtained from EM images and the structural constraint that corresponds to the salt bridge formed between D23 and K28 are required to deduce a unique molecular conformation for the bend region [57].

## 6.2 Backbone Psi Angle Determination

A direct determination of the backbone  $\psi$  angle can be obtained by the tensor correlation of the  $N_{(i)}-C^\alpha_{(i)}$  and  $C'_{(i)}-N_{(i+1)}$  vectors. One possibility is to excite the DQ coherence between  $C^\alpha_{(i)}$  and  $C'_{(i)}$  and then let the DQ coherence evolve under the influence of the heteronuclear  $^{13}\text{C}-^{15}\text{N}$  dipole–dipole interaction [181, 182]. The virtue of this design is that it can be easily combined with other resolution enhancement technique such as INADEQUATE [183]. Alternatively, the magnetization of  $C'_{(i)}$  dephased under the  $^{13}\text{C}-^{15}\text{N}$  dipolar coupling can be transferred to  $C^\alpha_{(i)}$  for another period of  $^{13}\text{C}-^{15}\text{N}$  dipolar dephasing [183]. This idea can be combined with the NCOCA experiment so that the superior resolution provided by the  $C^\alpha_{(i)}-N_{(i+1)}$  correlation could be exploited. The overall efficiency, however, is relatively low due to the use of two polarization-transfer steps, viz.  $^{15}\text{N} \rightarrow ^{13}\text{C}$  and  $^{13}\text{C} \rightarrow ^{13}\text{C}$  [183]. In comparison with the  $C'_{(i)}-C'_{(i+1)}$  techniques, the advantage of the  $N_{(i)}-C^\alpha_{(i)}-C'_{(i)}-N_{(i+1)}$  is that multiple  $\psi$  angles can be obtained from a uniformly labeled system [183]. Note that this so-called NCCN experiment cannot distinguish the sign of  $\psi$  and the most sensitive region is  $|\psi|$  equal to  $140-180^\circ$  [181]. To remove the sign ambiguity in  $\psi$ , one can resort to the correlation experiments of different symmetries such as  $H^\alpha_{(i)}-C^\alpha_{(i)}-N_{(i+1)}-H^N_{(i+1)}$  [184]. Strictly speaking, the correlation of the  $H^\alpha_{(i)}-C^\alpha_{(i)}$  and  $N_{(i+1)}-H^N_{(i+1)}$  vectors would depend on both the backbone  $\psi$  and  $\omega$  angles, but the deviation of  $\omega$  from the ideal values, i.e.,  $180^\circ$  for *trans* and  $0^\circ$  for *cis* conformations, should be very small in most cases. The above pulse frameworks are very general and different heteronuclear or homonuclear dipolar recoupling schemes can be incorporated in them for the backbone or side-chain torsion angle determinations [184]. The NCCN technique has been applied to study the backbone  $\psi$  angles of the GNNQQNY fibrils [25]. The results indicate that there is a localized non- $\beta$ -sheet structure at residue N8 in one of the three fibril conformers.

All the techniques we have discussed thus far for  $\psi$  determination require isotopic labeling of two consecutive residues. Nevertheless, it has been demonstrated that the backbone torsion  $\psi$  angle can be determined within a single  $^{13}\text{C}$  uniformly-labeled residue [185, 186]. The method, with the acronym RACO for relayed anisotropy correlation, comprises three basic modules, viz. the CSA recoupling of  $\text{C}'$ , the polarization transfer from  $\text{C}'$  to  $\text{C}^\alpha$ , and the heteronuclear  $^{13}\text{C}^\alpha$ - $^1\text{H}^\alpha$  dipolar recoupling [186]. That is, the backbone torsion  $\psi$  angle can be determined by correlating the carbonyl  $^{13}\text{C}$  chemical shift and the  $^{13}\text{C}^\alpha$ - $^1\text{H}^\alpha$  dipolar tensors within a single  $^{13}\text{C}$  uniformly-labeled residue. In its original implementation, RACO requires the acquisition of a series of 2D spectra under the heteronuclear dipolar recoupling condition and therefore is not applicable for systems with multiple uniformly  $^{13}\text{C}$  labeled residues. This limitation of RACO can be easily alleviated by separating the heteronuclear dipolar recoupling and the  $t_2$  acquisition periods, and by choosing recoupling pulse sequences designed for fast MAS [187]. However, without a detailed understanding of the basic principles of tensor correlation, it is not trivial to obtain the optimized implementation of RACO by trial and error because there are many different recoupling pulse sequences reported in the literature [63].

### 6.2.1 Echo Formation Between Two Correlated Anisotropic Interactions

In the following, we present a simple physical picture to illustrate some general features of the RACO approach. As mentioned above, the backbone  $\psi$  angle can be determined by correlating the  $\text{C}'$  chemical shift anisotropy and the  $\text{C}^\alpha$ - $\text{H}^\alpha$  dipolar interaction. Both interactions are anisotropic, i.e., the NMR signal evolving under the influence of either interaction will decay (or dephase) to zero in a powder sample. After the polarization transfer between  $\text{C}'$  and  $\text{C}^\alpha$ , the signal dephased in the first period may be partially refocused in the second period. The extent of the “echo” formation depends on whether the orientation dependence of the average Hamiltonians during the CSA and dipolar recoupling periods are in close resemblance [188]. In other words, the “echo” amplitude depends on: (1) the orientation dependence of the average Hamiltonian; (2) the durations of the two dephasing periods; (3) the relative orientation of the two internal interactions, which is implicitly related to the backbone  $\psi$  angle. When the recoupling pulse sequences for the CSA and the heteronuclear dipolar interactions are  $\gamma$ -encoded where the spatial parts  $m = 2$  are selected, the extent of the resemblance of the two average Hamiltonians has a strong dependence on the  $\psi$  angle, and one could then accurately determine the  $\psi$  angle by comparing the experimental echo amplitude and the results simulated based on the model spin system, which is usually set as  $\text{C}'$ - $\text{C}^\alpha$ - $\text{H}^\alpha$ . For convenience, experimentally we chose to use the FSLG technique which is a non- $\gamma$ -encoded sequence for heteronuclear dipolar recoupling. Nevertheless,  $\gamma$ -encoded sequences such as  $R18_2^5$  should be a good alternative option [108, 189]. Furthermore, to ensure the closest resemblance of the two average Hamiltonians, the homonuclear polarization transfer inserted



between the two recoupling periods should be isotropic. That is, the R-TOBSY sequence is a favorable choice for the homonuclear polarization transfer in the present context.

The experimental strategy discussed above was applied to determine the dihedral angle of uniformly  $^{13}\text{C}$  and  $^{15}\text{N}$  labeled L-alanine and N-acetyl-D,L-valine (NAV) samples. The  $^{13}\text{C}' \rightarrow \text{C}^\alpha$  peak intensities of three separate experiments corresponding to zero, one, and two complete cycles of CSA recoupling were measured while the dipolar recoupling period was fixed at three rotor periods [188]. The experimental data were normalized by the first data point (no CSA recoupling) and then compared with the numerical simulations carried out in the same fashion as discussed earlier. Due to the symmetry properties of the  $\text{C}'$  CSA and the  $\text{C}^\alpha\text{--H}^\alpha$  dipolar interactions, the plot of squared deviations ( $\chi^2$ ) between experimental and simulation data will have reflection symmetries about  $-150$ ,  $-60$ ,  $30$ , and  $120^\circ$  [186]. Minimum  $\chi^2$  values for L-alanine and NAV occur at  $\psi$  equal to  $160$  ( $161.5$ ) and  $175$  ( $178.2$ ) $^\circ$ , respectively, where the bracketed values correspond to the crystallographic data obtained by diffraction techniques [190, 191].

For the fibril samples formed by the H1 fragment of the Syrian hamster prion protein (SHPrP<sub>109–122</sub>, Ac-MKHMAGAAAAGAVV-NH<sub>2</sub>), the backbone  $\psi$  angles of the alanine residues in the AGAAAAGA region were determined by the tensor correlation method based on the RACO approach [52]. The  $\text{C}'$  CSA of A113 was characterized by the ROCSA incorporated with the  $\text{C}^\alpha$ -detection scheme [164] and it was assumed that the  $\text{C}'$  CSAs of all the alanine residues with  $\beta$ -strand conformation are approximately the same. Additional simulations show that the  $\psi$  angle determination is indeed not sensitive to the  $\text{C}'$  CSA. As a matter of the inherent symmetry of the tensors being correlated, there are two set of  $\psi$  angles which have the best agreement with the experimental data. One is in the range of  $75\text{--}100^\circ$ , whereas another one is in the  $\beta$ -sheet region. In this particular case, the secondary chemical shift ( $\delta - \delta_{\text{random}}$ ) data have shown that the AGAAAAGA region has the  $\beta$ -sheet conformation. Consequently, the  $\psi$  angles of the palindrome region were obtained with high precision, which had been used as the benchmark data for the subsequent molecular dynamics simulations [52].

### 6.3 Backbone Phi Angle Determination

The backbone  $\phi$  angle can be determined by the correlation of the  $\text{N--H}^\text{N}$  and  $\text{C}^\alpha\text{--H}^\alpha$  dipolar tensors [184, 192, 193]. The strategy of the earliest attempt is to create the  $^{15}\text{N}\text{--}^{13}\text{C}$  multiple-quantum coherence by REDOR and then let the coherence evolve under the scaled heteronuclear dipole–dipole interaction generated by MREV-8 [193]. As the technique of MREV-8 is designed for applications under static conditions, the phase evolution will be modulated by MAS. In other words, the dipolar dephasing during the first half of the rotor period will be refocused in the second half. Consequently, the spinning frequency must be less than 3 kHz so that the dephasing period is long enough to reveal the angular

dependence on  $\phi$  with sufficient resolution. As a logical extension of the original approach, it has been shown that the effective dephasing time of MREV-8 can be lengthened by insertion of rotor-synchronized  $\pi$  pulses in the  $^{13}\text{C}$  or  $^{15}\text{N}$  channels [192]. The idea is quite similar to REDOR because the average Hamiltonian of the heteronuclear dipole–dipole interaction generated by MREV-8 has the operator form of  $I_z S_z$  [193]. Consequently, the double coupling scheme can be applied under moderate spinning condition as long as the quasi-static approximation is still valid (ca. 10 kHz). For higher spinning frequency, the time modulation of the spatial part of the Hamiltonian (due to MAS) will interfere with the averaging process of MREV-8 in the spin part. That is, the averaging of the undesired homonuclear dipole–dipole interaction will become less effective. Because the one-bond dipolar coupling constant of  $\text{N}-\text{H}^{\text{N}}$  is smaller than that of  $\text{C}^{\alpha}-\text{H}^{\alpha}$  by approximately a factor of 2, the correlation of the two tensors will have a stronger dependence on the  $\phi$  angle when the dipolar dephasing period of  $\text{N}-\text{H}^{\text{N}}$  is doubled compared with that of  $\text{C}^{\alpha}-\text{H}^{\alpha}$ . This double coupling scheme has been realized by preparing two separate dephasing periods for the corresponding antiphase signals [192].

Taking the MREV-8 as a basic  $C$  element (duration =  $\tau_r/5$ ), one can generate a  $\gamma$ -encoded [194] version of MREV-8 by concatenating the five  $C$  elements with an rf phase set equal to  $k \times 2\pi/5$ , where  $k = 0-4$  [107]. The averaged Hamiltonian calculated to the lowest order for this so-called T-MREV method has the following form:

$$\bar{H}_{IS} = \{\kappa \bar{\omega}_{m=-1} I_+ + \kappa^* \bar{\omega}_{m=+1} I_-\} S_z, \quad (21)$$

where  $I_{\pm}$  denote the spin operators for protons,  $\kappa$  is the scaling factor of the pulse sequence, and  $\bar{\omega}_m$  denotes the spatial part of the average Hamiltonian [107]. The advantage of (21) is that the time dependence of both the spatial and spin parts has been considered and therefore the dephasing of the magnetization is cumulative over the whole irradiation period. As the T-MREV is constructed based on MREV-8, its application is also limited to spinning frequency under 10 kHz. This drawback can be alleviated by using recoupling sequence such as  $R18_2^5$  [108, 189]. In general, the use of  $\gamma$ -encoded sequences for the heteronuclear dipolar recoupling requires a proper account of the different  $T_2$  relaxation rates of the  $I$  and  $S$  states [107]. Based on T-MREV, a 3D  $^1\text{H}-^{15}\text{N}-^{13}\text{C}-^1\text{H}$  dipolar chemical shift experiment has been constructed for the  $\phi$  angle determination as shown in Fig. 13. In fact, the same experimental framework can be used for the  $\psi$  angle determination by the  $\text{H}^{\alpha}_{(i)}-\text{C}^{\alpha}_{(i)}-\text{N}_{(i+1)}-\text{H}^{\text{N}}_{(i+1)}$  correlation [184].

The molecular structure of the amyloid fibrils formed by fragment 105–115 of transthyretin (TTR<sub>105–115</sub>, YTIAALLSPTS) has been characterized by solid-state NMR. The fibril backbone structure was first established based on the TALOS analysis of the  $^{15}\text{N}$  and  $^{13}\text{C}$  chemical shifts [89]. Using the correlation experiments of  $\text{H}^{\text{N}}_{(i)}-\text{N}_{(i)}-\text{C}^{\alpha}_{(i)}-\text{H}^{\alpha}_{(i)}$ ,  $\text{H}^{\alpha}_{(i)}-\text{C}^{\alpha}_{(i)}-\text{N}_{(i+1)}-\text{H}^{\text{N}}_{(i+1)}$ , and  $\text{N}_{(i)}-\text{C}^{\alpha}_{(i)}-\text{C}'_{(i)}-\text{N}_{(i+1)}$ , a total of 41 constraints on 19 backbone torsion angles have been obtained in a

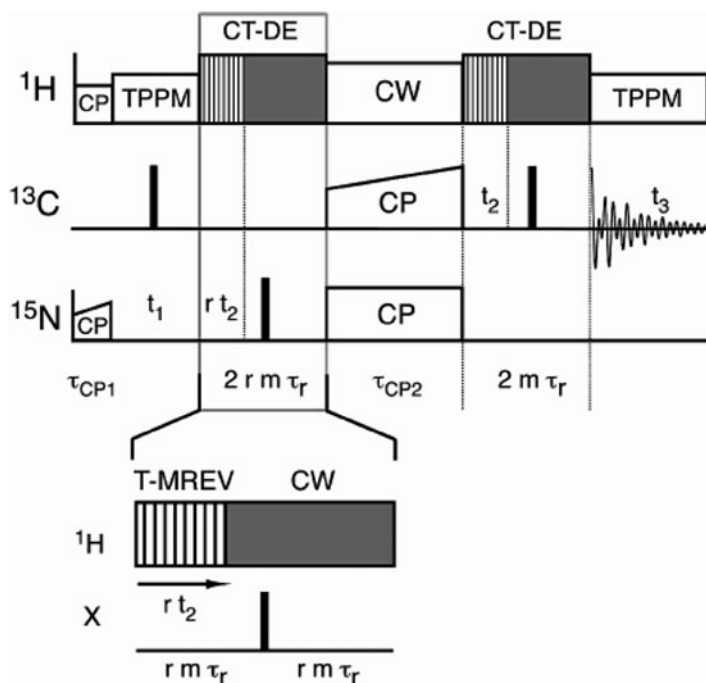


**Fig. 13** Pulse sequence for the 3D  $^1\text{H}$ - $^{15}\text{N}$ - $^{13}\text{C}$ - $^1\text{H}$  dipolar chemical shift experiment to constrain backbone and side-chain torsion angles. Polarization was transferred from  $^1\text{H}$  to  $^{15}\text{N}$  via ramped CP, followed by  $^{15}\text{N}$  chemical shift evolution during  $t_1$ . The period  $rt_2$  was a constant time dipolar recoupling period, composed of an integer number of rotor periods during which T-MREV is applied to the  $^1\text{H}$  spins. Polarization was subsequently transferred from  $^{15}\text{N}$  to  $^{13}\text{C}$  by amplitude-ramped SPECIFIC CP, and a second constant time T-MREV recoupling period,  $t_2$ , was applied to the transverse  $^{13}\text{C}$  coherences. Signal acquisition occurred during the period  $t_3$ . The ratio of  $^1\text{H}$ - $^{15}\text{N}$  to  $^1\text{H}$ - $^{13}\text{C}$  dipolar evolution ( $r$ ) was a fixed integer value, optimally 2. *Narrow and wide solid rectangles* represent  $\pi/2$  and  $\pi$  pulses, respectively. The phase cycling scheme can be found in the original figure and caption. (Figure and caption adapted from [184]. Copyright 2002 American Chemical Society)

subsequent study [104]. In addition, the torsion angles of most side chains have been constrained by the long-range C-N distances obtained by the 3D  $z$ -filtered TEDOR. Overall, a high-resolution structure of TTR<sub>105-115</sub> in the fibrillar state has been obtained [104], from which there are two interesting findings. First, the conformations of the backbone and side chains are very close to the regions of minimum intramolecular energy. Apparently, no significant energy barrier is present regarding to the conformational change of the monomer during the fibrillization of TTR<sub>105-115</sub>. Second, the residues P113 and T114 have adopted the  $\beta$ -sheet conformation, although the restricted  $\phi$  angle of proline precludes the formation of regular intermolecular hydrogen bondings at the sites of P113 and T114.

## 7 Conclusion and Outlook

Thanks to the pioneering works of many research groups, solid-state NMR is now a well established spectroscopy for the study of biological solids, particularly for those with inherent structural disorder such as amyloid fibrils. We have provided an overview of a rather complete set of NMR techniques which have developed for samples prepared by chemical synthesis or protein expression. There are many different ways to present the materials discussed in this review. We hope that the way we have chosen can give a snapshot of some facets of the very exciting discipline of biological solid-state NMR spectroscopy. In spite of the success of solid-state NMR as a tool in biological study, it is not yet a “mature” technique and there is much room for further development. Below we will speculate on a few possibilities from our own perspective.

To maximize the information content for each sample, the isotopic labeling scheme is preferred to be the uniform one. Because long-range contacts are the most important structural constraints, which can only be probed by dipolar-based techniques, further development in the suppression of the dipolar truncation effect and frequency-selective techniques is highly desirable for uniformly labeled samples. Polarization transfer between  $^{13}\text{C}$  and  $^{15}\text{N}$  is the key step in many pulse sequences. Techniques such as proton assisted insensitive nuclei cross polarization (PAIN-CP) [195] are promising candidates for the design of more efficient heteronuclear correlation experiments. Determination of backbone and side-chain torsion angles is always an important issue in solid-state NMR. Although some very useful techniques have been developed as discussed in this review, it is worthwhile to search for the possibility to characterize uniquely the  $\phi$  and  $\psi$  angles in a singly uniformly labeled residue. It can be envisioned that other tensor correlation techniques such as  $\text{C}^{\alpha}\text{H}-\text{C}'\text{N}$  [196] and  $\text{NH}^{\text{N}}-\text{NH}^{\text{N}}$  [197], which are not covered in this review, may find fruitful applications. A research area which is of great interest is the regime of very fast MAS ( $\geq 40$  kHz). Recoupling techniques developed for this regime are presumably less susceptible to the higher-order effects. As discussed in the chapter by Nielsen et al. [201] the optimal control theory has opened up a new avenue for the design of pulse sequence. The optimal control software has been implemented in the open-source SIMPSON package [198], which may be used to optimize the performance of many existing recoupling techniques. The importance of  $^{14}\text{N}$  is clearly underrepresented in biological NMR. Nevertheless, some promising techniques have been reported in the literature as discussed in the chapter by Fernandez and Pruski [199]. Needless to say, dynamic nuclear polarization (DNP) is an exciting option for signal enhancement in the NMR studies of biological samples [200]. All in all, it can be safely concluded that biological solid-state NMR will remain as a vibrant field for many years to come.

**Acknowledgment** This work was supported by the National Science Council of Taiwan. I would like to take this opportunity to thank Dr. Robert Tycko (NIH, Bethesda, USA) for introducing me to the field of amyloid fibrils. I also thank my former students Yun Mou, John Chin-Hao Chao, Tim Wen-Tin Tsai, Shin-Wen Lee, Ni-Shian Lin, Fang-Chieh Chou, Hsin-Mei Cheng, Wen-Chi Chu,

Yun-Ju Tang, Huei-Ying Lian, Hsin-Kuan Lee, Tzu-Hsueh Huang, and Yuan-Chi Huang for their many contributions in our own study of amyloid fibrils.

## References

1. Dobson CM (2003) *Nature* 426:884
2. Chiti F, Dobson CM (2006) *Annu Rev Biochem* 75:333
3. Spencer RGS, Halverson KJ, Auger M, McDermott AE, Griffin RG, Lansbury PT (1991) *Biochemistry* 30:10382
4. Tycko R (2006) *Q Rev Biophys* 39:1
5. Heise H (2008) *ChemBioChem* 9:179
6. Tycko R (2000) *Curr Opin Chem Biol* 4:500
7. Tycko R (2001) *Annu Rev Phys Chem* 52:575
8. Tycko R (2003) *Biochemistry* 42:3151
9. Tycko R (2003) *Prog Nucl Magn Reson Spectrosc* 42:53
10. Tycko R, Ishii Y (2003) *J Am Chem Soc* 125:6606
11. Tycko R (2004) *Curr Opin Struct Biol* 14:96
12. Naito A, Kawamura I (2007) *Biochim Biophys Acta* 1768:1900
13. Lansbury PT, Costa PR, Griffiths JM, Simon EJ, Auger M, Halverson KJ, Kocisko DA, Hendsch ZS, Ashburn TT, Spencer RGS et al (1995) *Nat Struct Biol* 2:990
14. Griffiths JM, Ashburn TT, Auger M, Costa PR, Griffin RG, Lansbury PT (1995) *J Am Chem Soc* 117:3539
15. Costa PR, Kocisko DA, Sun BQ, Lansbury PT, Griffin RG (1997) *J Am Chem Soc* 119:10487
16. Raleigh DP, Levitt MH, Griffin RG (1988) *Chem Phys Lett* 146:71
17. Levitt MH, Raleigh DP, Creuzet F, Griffin RG (1990) *J Chem Phys* 92:6347
18. Gregory DM, Benzinger TLS, Burkoth TS, Miller-Auer H, Lynn DG, Meredith SC, Botto RE (1998) *Solid State Nucl Magn Reson* 13:149
19. Walsh P, Simonetti K, Sharpel S (2009) *Structure* 17:417
20. Sawaya MR, Sambashivan S, Nelson R, Ivanova MI, Sievers SA, Apostol MI, Thompson MJ, Balbirnie M, Wiltzius JJW, McFarlane HT et al (2007) *Nature* 447:453
21. Ramachandran R, Ladizhansky V, Bajaj VS, Griffin RG (2003) *J Am Chem Soc* 125:15623
22. Costa PR, Sun BQ, Griffin RG (2003) *J Magn Reson* 164:92
23. Ramachandran R, Lewandowski JR, van der Wel PCA, Griffin RG (2006) *J Chem Phys* 124:214107
24. van der Wel PCA, Lewandowski JR, Griffin RG (2007) *J Am Chem Soc* 129:5117
25. van der Wel PCA, Lowandowski JR, Griffin RG (2010) *Biochemistry* 49:9457
26. Gregory DM, Mitchell DJ, Stringer JA, Kiihne S, Shiels JC, Callahan J, Mehta MA, Drobny GP (1995) *Chem Phys Lett* 246:654
27. Mehta MA, Gregory DM, Kiihne S, Mitchell DJ, Hatcher ME, Shiels JC, Drobny GP (1996) *Solid State Nucl Magn Reson* 7:211
28. Benzinger TLS, Gregory DM, Burkoth TS, Miller-Auer H, Lynn DG, Botto RE, Meredith SC (1998) *Proc Natl Acad Sci USA* 95:13407
29. Caporini MA, Bajaj VS, Veshtort M, Fitzpatrick A, MacPhee CE, Vendruscolo M, Dobson CM, Griffin RG (2010) *J Phys Chem B* 114:13555
30. Gregory DM, Wolfe GM, Jarvie TP, Shiels JC, Drobny GP (1996) *Mol Phys* 89:1835
31. Liu P, Ni R, Mehta AK, Childers WS, Lakdawala A, Pingali SV, Thiagarajan P, Lynn DG (2008) *J Am Chem Soc* 130:16867
32. Childers WS, Mehta AK, Ni R, Taylor JV, Lynn DG (2010) *Angew Chem Int Ed Engl* 49:4104

33. Karlsson T, Popham JM, Long JR, Oyler N, Drobny GP (2003) *J Am Chem Soc* 125:7394
34. Schmedt auf der Gunne J, Eckert H (1998) *Chem Eur J* 4:1762
35. Gullion T, Vega S (1992) *Chem Phys Lett* 194:423
36. Bennett AE, Ok JH, Griffin RG, Vega S (1992) *J Chem Phys* 96:8624
37. Bennett AE, Rienstra CM, Griffiths JM, Zhen WG, Lansbury PT, Griffin RG (1998) *J Chem Phys* 108:9463
38. Ishii Y (2001) *J Chem Phys* 114:8473
39. Bennett AE, Weliky DP, Tycko R (1998) *J Am Chem Soc* 120:4897
40. Waugh JS, Huber LM, Haeberle U (1968) *Phys Rev Lett* 20:180
41. Ishii Y, Balbach JJ, Tycko R (2001) *Chem Phys* 266:231
42. Balbach JJ, Petkova AT, Oyler NA, Antzutkin ON, Gordon DJ, Meredith SC, Tycko R (2002) *Biophys J* 83:1205
43. Petkova AT, Ishii Y, Balbach JJ, Antzutkin ON, Leapman RD, Delaglio F, Tycko R (2002) *Proc Natl Acad Sci USA* 99:16742
44. Antzutkin ON, Leapman RD, Balbach JJ, Tycko R (2002) *Biochemistry* 41:15436
45. Chan JCC, Oyler N, Yau WM, Tycko R (2005) *Biochemistry* 44:10669
46. Shewmaker F, Wickner RB, Tycko R (2006) *Proc Natl Acad Sci USA* 103:19754
47. Luca S, Yau WM, Leapman R, Tycko R (2007) *Biochemistry* 46:13505
48. Wickner RB, Dyda F, Tycko R (2008) *Proc Natl Acad Sci USA* 105:2403
49. Wasmer C, Lange A, Van Melckebeke H, Siemer AB, Riek R, Meier BH (2008) *Science* 319:1523
50. Lin NS, Chao JCH, Cheng HM, Chou FC, Chang CF, Chen YR, Chang YJ, Huang SJ, Chan JCC (2010) *Chem Eur J* 16:5492
51. Tycko R, Sciarretta KL, Orgel J, Meredith SC (2009) *Biochemistry* 48:6072
52. Lee SW, Mou Y, Lin S-Y, Chou F-C, Tseng W-H, Chen C-H, Yu SS-F, Lu C-YD, Chan JCC (2008) *J Mol Biol* 378:1142
53. Shewmaker F, Kryndushkin D, Chen B, Tycko R, Wickner RB (2009) *Biochemistry* 48:5074
54. Tycko R, Savtchenko R, Ostapchenko VG, Makarava N, Baskakov IV (2010) *Biochemistry* 49:9488
55. Tycko R (2007) *J Chem Phys* 126:064506
56. Bower PV, Oyler N, Mehta MA, Long JR, Stayton PS, Drobny GP (1999) *J Am Chem Soc* 121:8373
57. Antzutkin ON, Balbach JJ, Tycko R (2003) *Biophys J* 84:3326
58. Weitekamp DP (1983) In: Waugh JS (ed) *Advances in magnetic resonance*. Academic, New York, pp 111
59. Antzutkin ON, Balbach JJ, Leapman RD, Rizzo NW, Reed J, Tycko R (2000) *Proc Natl Acad Sci USA* 97:13045
60. Oyler NA, Tycko R (2002) *J Phys Chem B* 106:8382
61. Eden M, Brinkmann A, Luthman H, Eriksson L, Levitt MH (2000) *J Magn Reson* 144:266
62. Baldus M (2002) *Prog Nucl Magn Reson Spectrosc* 41:1
63. Schnell I (2004) *Prog Nucl Magn Reson Spectrosc* 45:145
64. Ramamoorthy A, Fujiwara T, Nagayama K (1993) *J Magn Reson A* 104:366
65. Baldus M, Meier BH (1996) *J Magn Reson A* 121:65
66. Baldus M, Iulucci RJ, Meier BH (1997) *J Am Chem Soc* 119:1121
67. Lesage A, Auger C, Caldarelli S, Emsley L (1997) *J Am Chem Soc* 119:7867
68. Verel R, van Beek J, Meier BH (1999) *J Magn Reson* 140:300
69. Lesage A, Bardet M, Emsley L (1999) *J Am Chem Soc* 121:10987
70. Heindrichs ASD, Geen H, Giordani C, Titman JJ (2001) *Chem Phys Lett* 335:89
71. Hardy EH, Verel R, Meier BH (2001) *J Magn Reson* 148:459
72. Chan JCC, Brunklaus G (2001) *Chem Phys Lett* 349:104
73. Hardy EH, Detken A, Meier BH (2003) *J Magn Reson* 165:208
74. Ernst M, Detken A, Bockmann A, Meier BH (2003) *J Am Chem Soc* 125:15807

75. Mueller LJ, Elliott DW, Leskowitz GM, Struppe J, Olsen RA, Kim K-C, Reed CA (2004) *J Magn Reson* 168:327
76. Duma L, Lai WC, Carravetta M, Emsley L, Brown SP, Levitt MH (2004) *ChemPhysChem* 5:815
77. Ishii Y, Ashida J, Terao T (1995) *Chem Phys Lett* 246:439
78. Yannoni CS, Kendrick RD (1981) *J Chem Phys* 74:747
79. Hughes CE, Luca S, Baldus M (2004) *Chem Phys Lett* 385:435
80. Mou Y, Chao JCH, Chan JCC (2006) *Solid State Nucl Magn Reson* 29:278
81. Mou Y, Chan JCC (2006) *Chem Phys Lett* 419:144
82. Lee YK, Kurur ND, Helmle M, Johannessen OG, Nielsen NC, Levitt MH (1995) *Chem Phys Lett* 242:304
83. Hohwy M, Jakobsen HJ, Eden M, Levitt MH, Nielsen NC (1998) *J Chem Phys* 108:2686
84. Paravastu AK, Tycko R (2006) *J Chem Phys* 124:194303
85. Hu KN, Tycko R (2009) *J Chem Phys* 131:045101
86. Gullion T, Schaefer J (1989) *J Magn Reson* 81:196
87. Gullion T (1998) *Concepts Magn Reson* 10:277
88. Gullion T, Vega AJ (2005) *Prog Nucl Magn Reson Spectrosc* 47:123
89. Jaroniec CP, MacPhee CE, Astrof NS, Dobson CM, Griffin RG (2002) *Proc Natl Acad Sci USA* 99:16748
90. Anderson RC, Gullion T, Joers JM, Shapiro M, Villhauer EB, Weber HP (1995) *J Am Chem Soc* 117:10546
91. Nelson R, Sawaya MR, Balbirnie M, Madsen AO, Riek C, Grothe R, Eisenberg D (2005) *Nature* 435:773
92. Jaroniec CP, Tounge BA, Herzfeld J, Griffin RG (2001) *J Am Chem Soc* 123:3507
93. Li Y, Wylie BJ, Rienstra CM (2006) *J Magn Reson* 179:206
94. Perutz MF (1996) *Curr Opin Struct Biol* 6:848
95. Perutz MF, Staden R, Moens L, Debaere I (1993) *Curr Biol* 3:249
96. Perutz MF, Pope BJ, Owen D, Wanker EE, Scherzinger E (2002) *Proc Natl Acad Sci USA* 99:5596
97. Wagner A, Luger P (2001) *J Mol Struct* 595:39
98. Gullion T, Baker DB, Conradi MS (1990) *J Magn Reson* 89:479
99. Bennett AE, Rienstra CM, Auger M, Lakshmi KV, Griffin RG (1995) *J Chem Phys* 103:6951
100. Sorensen OW, Eich GW, Levitt MH, Bodenhausen G, Ernst RR (1983) *Prog Nucl Magn Reson Spectrosc* 16:163
101. Oyler NA, Tycko R (2007) *Magn Reson Chem* 45:S101
102. Jaroniec CP, Filip C, Griffin RG (2002) *J Am Chem Soc* 124:10728
103. Helmus JJ, Surewicz K, Surewicz WK, Jaroniec CP (2010) *J Am Chem Soc* 132:2393
104. Jaroniec CP, MacPhee CE, Bajaj VS, McMahon MT, Dobson CM, Griffin RG (2004) *Proc Natl Acad Sci USA* 101:711
105. Bielecki A, Kolbert AC, de Groot HJM, Griffin RG, Levitt MH (1990) *Adv Magn Reson* 14:111
106. Takegoshi K, Nakamura S, Terao T (1999) *Chem Phys Lett* 307:295
107. Hohwy M, Jaroniec CP, Reif B, Rienstra CM, Griffin RG (2000) *J Am Chem Soc* 122:3218
108. Zhao X, Sudmeier JL, Bachovchin WW, Levitt MH (2001) *J Am Chem Soc* 123:11097
109. Szeverenyi NM, Sullivan MJ, Maciel GE (1982) *J Magn Reson* 47:462
110. Takegoshi K, Nakamura S, Terao T (2001) *Chem Phys Lett* 344:631
111. Takegoshi K, Nakamura S, Terao T (2003) *J Chem Phys* 118:2325
112. Morcombe CR, Gaponenko V, Byrd RA, Zilm KW (2004) *J Am Chem Soc* 126:7196
113. Verel R, Ernst M, Meier BH (2001) *J Magn Reson* 150:81
114. Leppert J, Ohlenschlager O, Gorchach M, Ramachandran R (2004) *J Biomol NMR* 29:167
115. Wasmer C, Soragni A, Sabate R, Lange A, Riek R, Meier BH (2008) *Angew Chem Int Ed Engl* 47:5839

116. Heise H, Celej MS, Becker S, Riede D, Pelah A, Kumar A, Jovin TM, Baldus M (2008) *J Mol Biol* 380:444
117. Wasmer C, Benkemoun L, Sabate R, Steinmetz MO, Coulary-Salin B, Wang L, Riek R, Saupe SJ, Meier BH (2009) *Angew Chem Int Ed Engl* 48:4858
118. Nielsen JT, Bjerring M, Jeppesen MD, Pedersen RO, Pedersen JM, Hein KL, Vosegaard T, Skrydstrup T, Otzen DE, Nielsen NC (2009) *Angew Chem Int Ed Engl* 48:2118
119. Helmus JJ, Surewicz K, Nadaud PS, Surewicz WK, Jaroniec CP (2008) *Proc Natl Acad Sci USA* 105:6284
120. Chimon S, Shaibat MA, Jones CR, Calero DC, Aizezi B, Ishii Y (2007) *Nat Struct Mol Biol* 14:1157
121. Siemer AB, Ritter C, Steinmetz MO, Ernst M, Riek R, Meier BH (2006) *J Biomol NMR* 34:75
122. Bayro MJ, Ramachandran R, Caporini MA, Eddy MT, Griffin RG (2008) *J Chem Phys* 128:11
123. De Paepe G, Bayro MJ, Lewandowski J, Griffin RG (2006) *J Am Chem Soc* 128:1776
124. Bayro MJ, Maly T, Birkett NR, MacPhee CE, Dobson CM, Griffin RG (2010) *Biochemistry* 49:7474
125. Debelouchina GT, Platt GW, Bayro MJ, Radford SE, Griffin RG (2010) *J Am Chem Soc* 132:10414
126. Nadaud PS, Helmus JJ, Hofer N, Jaroniec CP (2007) *J Am Chem Soc* 129:7502
127. Su Y, Mani R, Hong M (2008) *J Am Chem Soc* 130:8856
128. Nadaud PS, Helmus JJ, Kall SL, Jaroniec CP (2009) *J Am Chem Soc* 131:8108
129. Wickramasinghe NP, Parthasarathy S, Jones CR, Bhardwaj C, Long F, Kotecha M, Mehboob S, Fung LW, Past J, Samoson A, Ishii Y (2009) *Nat Methods* 6:215
130. Walsh P, Neudecker P, Sharpe S (2010) *J Am Chem Soc* 132:7684
131. Baldus M, Petkova AT, Herzfeld J, Griffin RG (1998) *Mol Phys* 95:1197
132. Petkova AT, Yau WM, Tycko R (2006) *Biochemistry* 45:498
133. Andronesi OC, Becker S, Seidel K, Heise H, Young HS, Baldus M (2005) *J Am Chem Soc* 127:12965
134. Heise H, Hoyer W, Becker S, Andronesi OC, Riedel D, Baldus M (2005) *Proc Natl Acad Sci USA* 102:15871
135. Siemer AB, Arnold AA, Ritter C, Westfeld T, Ernst M, Riek R, Meier BH (2006) *J Am Chem Soc* 128:13224
136. Lange A, Gattin Z, Van Melckebeke H, Wasmer C, Soragni A, van Gunsteren WF, Meier BH (2009) *ChemBioChem* 10:1657
137. Tycko R, Hu KN (2010) *J Magn Reson* 205:304
138. Cornilescu G, Delaglio F, Bax A (1999) *J Biomol NMR* 13:289
139. Shen Y, Delaglio F, Cornilescu G, Bax A (2009) *J Biomol NMR* 44:213
140. Lange A, Luca S, Baldus M (2002) *J Am Chem Soc* 124:9704
141. Seidel K, Eitzkorn M, Heise H, Becker S, Baldus M (2005) *ChemBioChem* 6:1638
142. Castellani F, van Rossum B, Diehl A, Schubert M, Rehbein K, Oschkinat H (2002) *Nature* 420:98
143. Ahmed M, Davis J, Aucoin D, Sato T, Ahuja S, Aimoto S, Elliott JI, Van Nostrand WE, Smith SO (2010) *Nat Struct Mol Biol* 17:561
144. Luhrs T, Ritter C, Adrian M, Riek-Loher D, Bohrmann B, Doeli H, Schubert D, Riek R (2005) *Proc Natl Acad Sci USA* 102:17342
145. Petkova AT, Leapman RD, Guo ZH, Yau WM, Mattson MP, Tycko R (2005) *Science* 307:262
146. Paravastua AK, Leapman RD, Yau WM, Tycko R (2008) *Proc Natl Acad Sci USA* 105:18349
147. Bayro Marvin J, Maly T, Birkett Neil R, Dobson Christopher M, Griffin Robert G (2009) *Angew Chem Int Ed* 48:5708



148. De Paepe G, Lewandowski JR, Loquet A, Bockmann A, Griffin RG (2008) *J Chem Phys* 129:245101
149. Ladizhansky V (2009) *Solid State Nucl Magn Reson* 36:119
150. Nieuwkoop AJ, Rienstra CM (2010) *J Am Chem Soc* 132:7570
151. Debelouchina GT, Platt GW, Bayro MJ, Radford SE, Griffin RG (2010) *J Am Chem Soc* 132:17077
152. Ritter C, Maddelein ML, Siemer AB, Luhrs T, Ernst M, Meier BH, Saupé SJ, Riek R (2005) *Nature* 435:844
153. Vilar M, Chou HT, Luhrs T, Maji SK, Riek-Loher D, Verel R, Manning G, Stahlberg H, Riek R (2008) *Proc Natl Acad Sci USA* 105:8637
154. Kheterpal I, Wetzel R (2006) *Acc Chem Res* 39:584
155. Hoshino M, Katou H, Yamaguchi K, Goto Y (2007) *Biochim Biophys Acta* 1768:1886
156. Svane ASP, Jahn K, Deva T, Malmendal A, Otzen DE, Dittmer J, Nielsen NC (2008) *Biophys J* 95:366
157. Liu SF, Mao JD, Schmidt-Rohr K (2002) *J Magn Reson* 155:15
158. Chan JCC, Tycko R (2003) *J Chem Phys* 118:8378
159. Levitt MH (2002) In: Grant DM, Harris RK (eds) *Encyclopedia of nuclear magnetic resonance*. Wiley, Chichester, pp 165
160. Chan JCC (2001) *Chem Phys Lett* 335:289
161. Chan JCC, Eckert H (2001) *J Chem Phys* 115:6095
162. Oldfield E (2002) *Annu Rev Phys Chem* 53:349
163. Wylie BJ, Rienstra CM (2008) *J Chem Phys* 128:052207
164. Mou Y, Chen PH, Lee SW, Chan JCC (2007) *J Magn Reson* 187:352
165. Tycko R, Dabbagh G (1991) *J Am Chem Soc* 113:9444
166. Robyr P, Meier BH, Fischer P, Ernst RR (1994) *J Am Chem Soc* 116:5315
167. Feng X, Lee YK, Sandstrom D, Eden M, Maisel H, Sebald A, Levitt MH (1996) *Chem Phys Lett* 257:314
168. Tycko R, Weliky DP, Berger AE (1996) *J Chem Phys* 105:7915
169. Weliky DP, Tycko R (1996) *J Am Chem Soc* 118:8487
170. Gregory DM, Mehta MA, Shiels JC, Drobny GP (1997) *J Chem Phys* 107:28
171. Blanco FJ, Tycko R (2001) *J Magn Reson* 149:131
172. Walling AE, Pargas RE, deDios AC (1997) *J Phys Chem A* 101:7299
173. Oas TG, Hartzell CJ, McMahon TJ, Drobny GP, Dahlquist FW (1987) *J Am Chem Soc* 109:5956
174. Oas TG, Hartzell CJ, Dahlquist FW, Drobny GP (1987) *J Am Chem Soc* 109:5962
175. Hartzell CJ, Whitfield M, Oas TG, Drobny GP (1987) *J Am Chem Soc* 109:5966
176. Teng Q, Iqbal M, Cross TA (1992) *J Am Chem Soc* 114:5312
177. Asakawa N, Kuroki S, Kurosu H, Ando I, Shoji A, Ozaki T (1992) *J Am Chem Soc* 114:3261
178. Kameda T, Takeda N, Kuroki S, Kurosu H, Ando S, Ando I, Shoji A, Ozaki T (1996) *J Mol Struct* 384:17
179. Takeda N, Kuroki S, Kurosu H, Ando I (1999) *Biopolymers* 50:61
180. Saito H, Ando I, Ramamoorthy A (2010) *Prog Nucl Magn Reson Spectrosc* 57:181
181. Costa PR, Gross JD, Hong M, Griffin RG (1997) *Chem Phys Lett* 280:95
182. Feng X, Eden M, Brinkmann A, Luthman H, Eriksson L, Graslund A, Antzutkin ON, Levitt MH (1997) *J Am Chem Soc* 119:12006
183. Ladizhansky V, Jaroniec CP, Diehl A, Oschkinat H, Griffin RG (2003) *J Am Chem Soc* 125:6827
184. Rienstra CM, Hohwy M, Mueller LJ, Jaroniec CP, Reif B, Griffin RG (2002) *J Am Chem Soc* 124:11908
185. Schmidt-Rohr K (1996) *J Am Chem Soc* 118:7601
186. Ishii Y, Terao T, Kainosho M (1996) *Chem Phys Lett* 256:133
187. Chan JCC, Tycko R (2003) *J Am Chem Soc* 125:11828
188. Mou Y, Tsai TWT, Chan JCC (2007) *Solid State Nucl Magn Reson* 31:72

189. Zhao X, Eden M, Levitt MH (2001) *Chem Phys Lett* 342:353
190. Lehmann MS, Koetzle TF, Hamilton WC (1972) *J Am Chem Soc* 94:2657
191. Carroll PJ, Stewart PL, Opella SJ (1990) *Acta Crystallogr Sect C Cryst Struct Commun* 46:243
192. Hong M, Gross JD, Rienstra CM, Griffin RG, Kumashiro KK, Schmidt-Rohr K (1997) *J Magn Reson* 129:85
193. Hong M, Gross JD, Griffin RG (1997) *J Phys Chem B* 101:5869
194. Nielsen NC, Bildsoe H, Jakobsen HJ, Levitt MH (1994) *J Chem Phys* 101:1805
195. Lewandowski JR, De Paepe G, Griffin RG (2007) *J Am Chem Soc* 129:728
196. Ladizhansky V, Veshtort M, Griffin RG (2002) *J Magn Reson* 154:317
197. Reif B, Hohwy M, Jaroniec CP, Rienstra CM, Griffin RG (2000) *J Magn Reson* 145:132
198. Bak M, Rasmussen JT, Nielsen NC (2000) *J Magn Reson* 147:296
199. Fernandez C, Pruski M (2011) Probing quadrupolar nuclei by solid-state NMR spectroscopy: recent advances. *Top Curr Chem*. doi:10.1007/128\_2011\_141
200. Griffin RG, Prisner TF (2010) *Phys Chem Chem Phys* 12:5737
201. Nielsen NC, Strassø LA, Nielsen AB (2011) *Top Curr Chem* DOI: 10.1007/128\_2011\_129



<http://www.springer.com/978-3-642-24802-3>

Solid State NMR

Chan, J.C.C. (Ed.)

2012, XII, 320 p., Hardcover

ISBN: 978-3-642-24802-3